Optimal Ranking Regime Analysis of TreeFlow Dendrohydrological Reconstructions.

S. A. Mauget

{USDA-ARS Plant Stress and Water Conservation Laboratory, Lubbock, TX }

Correspondence to: S.A. Mauget (Steven.Mauget@.ars.usda.gov)

Abstract

The Optimal Ranking Regime (ORR) method was used to identify 6-100 year time windows containing significant ranking sequences in 55 western U.S. streamflow reconstructions, and reconstructions of the level of the Great Salt Lake and San Francisco Bay salinity during 1500-2007. The method's ability to identify optimally significant and non-overlapping runs of low and high rankings allows it to re-express a reconstruction time series as a simplified sequence of regime segments marking intra- to multi-decadal (IMD) periods of low or high streamflow, lake level, or salinity. Those ORR sequences, referred to here as Z-lines, can be plotted to identify consistent regime patterns in the analysis of numerous reconstructions. The Z-lines for the 57 reconstructions evaluated here show a common pattern of IMD cycles of drought and pluvial periods during the late 16th and 17th centuries, a relatively dormant period during the 18th century, and the reappearance of alternating dry and wet IMD periods during the 19th and early 20th centuries. Although this pattern suggests the possibility of similarly active and inactive oceanic modes in the North Pacific and North Atlantic, such centennial-scale patterns are not evident in the ORR analyses of reconstructed Pacific Decadal

Oscillation (PDO), El Niño-Southern Oscillation, and North Atlantic seas-surface temperature variation. But given the inconsistency in the analyses of four PDO reconstructions the possible role of centennial-scale oceanic mechanisms is uncertain. In future research the ORR method might be applied to climate reconstructions around the Pacific Basin to try to resolve this uncertainty. Given its ability to compare regime patterns in climate reconstructions derived using different methods and proxies, the method may also be used in future research to evaluate long-term regional temperature reconstructions.

1 Introduction

Since the first attempts at tree-ring dating analysis over the western U.S. focus has shifted from questions centered on the past to questions related to current and future water management. Whereas the early emphasis was on the dating of prehistoric native American structures in the U.S. southwest (Nash 1999; Creasman et al. 2012), subsequent work has tried to better estimate hydrological variability over important watershed areas of the arid American west. Although the first streamflow reconstructions based on tree-ring data were conducted in the 1930s (see Meko and Woodhouse, 2011 for a review), the growth of western population and agricultural production centers in the latter half of the 20th century spurred demand for better estimates of hydrological variability than were available from gauged streamflow data records.

A leading example of the re-assessment of a key western U.S. water resource was Stockton and Jacoby's (1976) reconstruction of Colorado River flow at Lee's Ferry Arizona. The Colorado River Compact (MacDonnell et al. 1995; Hundley 2009) was based on a 16.4 million acre-feet (maf) per year Lee's Ferry flow estimate derived from relatively brief gauge

47 records from the period immediately preceding the Compact's 1922 drafting. However,
48 Stockton and Jacoby's 1512-1961 flow reconstruction varied about an average level of 13.5
49 maf. As a result, the Compact's equal 7.5 maf division of flow between the upper and lower
50 Colorado basins over-allocated the river's water. Given the experience of more recent western
51 U.S. drought conditions (e.g. Pagano et al., 2004, Woodhouse and Lukas 2006a; Woodhouse
52 et al. 2006), and doubts that the variability in centennial-scale gauge records reflect what
53 water managers might expect in the near future, the current demand for more representative
54 records of hydro-climate is particularly clear regarding the intensity, duration, and recurrence
55 of drought (Rice et al 2009).
56 In meeting the need for extended proxy records streamflow reconstructions have been
57 conducted over a number of western watershed regions including the upper Snake (Wise
58 2010), the upper Colorado (Woodhouse and Lukas, 2006a; Woodhouse et al., 2006; Meko et
59 al. 2007; Gray et al 2011), the South Platte (Woodhouse and Lukas, 2006a), the Rio Grande
60 (Margolis et al. 2011), the Great Salt Lake (Bekker et al. 2014; DeRose et al. 2014) and
61 California's central valley (Meko et al. 2001). The results of many of these reconstructions
62 have been made available via the TreeFlow web data resource (http://treeflow.info). The
63 amount of data currently available from treeflo.info – 54 TreeFlow reconstructions are
64 evaluated here in addition to flow and lake level reconstructions from other sources – presents
65 both opportunities and challenges. The analysis of multiple reconstructions allows for the
66 possibility of detecting patterns of common pluvial and drought regimes in the pre-
67 instrumental period. However, objectively and consistently identifying these regime periods,
68 and presenting the results in a way that can expose consistent patterns of variation may require
69 new approaches to time series analysis.

One commonly used method to test for regimes in multi-century proxy climate records is runs analysis (Meko et al. 1995,2007; Biondi et al., 2002, 2005; Gray et al. 2011; Bekker et al. 2014). This approach defines the run duration of extreme flow periods as the number of consecutive high or low flow years above or below a specified flow threshold. The sum of those flow departures above or below that threshold is referred to as the run magnitude, while the average departure over the run's duration, i.e. the run's magnitude divided by it's duration, is the run intensity (Dracup et al 1980; Biondi et al. 2002). However, as noted by Gray et al. (2011) and Meko and Woodhouse (2011), a basic problem with this method is that single years exceeding the threshold in the midst of otherwise extended runs results in the definition of two individual runs. Also, a drought or pluvial period's magnitude and intensity are dependent on the choice of a subjectively chosen threshold. Thus while runs analysis can provide information about the magnitude and duration of anomalous flow events in a reconstructed streamflow record, it's results can be dependent on the choice of threshold and may not provide the most robust estimates of event duration.

A second method that can be used to detect regime periods in climate records is intervention analysis. As described by Box and Tiao (1975) and used by Mantua et al. (1997), intervention analysis involves forming stochastic models that account for the influence of events, or interventions, that lead to abrupt changes in a time series. This iterative process of model identification, fitting, and diagnostic checking assumes prior knowledge of the timing of intervention events. When that timing is not known, candidate regime shifts have been identified via two-sample t-tests to detect significant shifts in 15 year sample means before and after each year in a time series (Gedalof and Smith 2001; D'Arrigo et al. 2005).

92 In previous work the Optimal Ranking Regime (ORR) method has been used to identify
93 significant intra- to multi-decadal (IMD) periods in U.S. temperature, precipitation, and
94 streamflow during the instrumental period (Mauget 2003a,b 2004; Cordero et al. 2011;
95 Mauget and Cordero 2014a,b), and in reconstructed records of South American snowpack
96 based on tree-ring data (Masiokas et al. 2012). This approach ranks a time series' data values,
97 samples those rankings over moving time windows, and then calculates Mann-Whitney U and
98 Z statistics for each running sample. Conducting this sampling process over running time
99 windows allows for testing every possible ranking sequence occurring over a fixed window
100 duration. By repeating this running sampling using windows of varying widths, the process
101 exhaustively samples the ranking sequences in a time series over a range of time scales.
102 Comparing the magnitudes of the resulting Z statistics for all the ranking samples allows the
103 method to objectively identify a time series' most significant sequences of low or high
104 rankings. The ORR algorithm's simple output – a time series' most significant, non-
105 overlapping ranking regimes - makes it possible to graphically identify common drought or
106 pluvial regime patterns in the analyses of many hydroclimate reconstructions. Using this
107 graphic approach here may allow for a 'big picture' of the reconstructed IMD flow regimes in
108 the current TreeFlow data during 1500-2007. Given that features of climate reconstructions
109 might be sensitive to choices of modeling methodology (Hidalgo et al. 2000; Woodhouse et
110 al. 2006), this may also have a corroborative effect in showing common regime patterns in
111 reconstructions produced by investigators using different methods.
112 In the following Section 2 describes the streamflow, lake level, and salinity reconstruction
113 data evaluated here. Section 3 explains the ORR method and demonstrates it on Colorado
114 River at Lee's Ferry reconstructed annual flow values during 1500-2005. Section 4 presents

115 the results of the ORR approach on all 57 reconstructed data series during 1500-2010.
116 Section 5 summarizes and discusses Section 4's results, outlines the advantages and
117 disadvantages in using the ORR approach in evaluating reconstructed climate series, and
118 proposes possible future research to apply the method to climate reconstructions around the
119 Pacific basin.

120 **2 Data**

121 The dendrohydrological data evaluated here (Table 1) includes 55 streamflow reconstructions,
122 and reconstructions of Great Salt Lake level (DeRose et al. 2014) and San Francisco Bay
123 salinity (Stahle et al. 2001). Figure 1 shows the locations of the USGS gauge stations
124 associated with each flow reconstruction and the general locations of San Francisco Bay and
125 the Great Salt Lake. Although the Sacramento-Four reconstruction (Meko et al. 2001) was
126 derived as the sum of four streamflow components in the Sacramento River watershed, its
127 location is marked at the junction of the Sacramento and American Rivers. The Stahle et al.
128 (2001) salinity data and all but two of the streamflow records were obtained from
129 treeflow.info. Reconstructed flow values for the Columbia River at The Dalles (Gedalof et al.
130 2004) was obtained via personal communication with Z'ev Gedalof. The Weber River flow
131 near Oakley, Utah (Bekker et al 2014) and Great Salt Lake Level data was obtained from
132 Matthew Bekker and Justin DeRose of the Wasatch Dendroclimatology Research Group. Of
133 Table 1's 57 reconstructions the shortest is Gedalof et al.'s (2004) record of annual
134 Columbia River flow (238 years), while the longest is Meko et al.'s (2007) Colorado River
135 flow at Lee's Ferry AZ reconstruction (1241 years). In the following these stations will be
136 referred to by their Table 1 reconstruction number, i.e., R1, R2,…R57.

137 Given the goal of detecting patterns of intra-decadal to centennial-scale hydrological regimes
138 over the western U.S., a network of streamflow gauge stations with a more uniform
139 geographic distribution than that found in Fig. 1 would be ideal. However, more than 1/3rd of
140 Fig. 1's stations (R19-R36) are concentrated in northern Colorado over the upper watersheds
141 of the Colorado and South Platte rivers. More than 3/4^{ths} (R4-R47) are located in three states
142 in the interior western U.S. – Wyoming, Utah and Colorado (WY-UT-CO). This in part due to
143 the demand of western water managers for better estimates of drought duration and recurrence
144 in key watershed areas of the U.S. central Rockies (e.g., Woodhouse and Lukas 2006a,b,c).
145 Another source of data redundancy is the repetition of reconstructions at gauge stations by
146 different investigators. Flow records for the Green River at Green River, Wyoming (R13,
147 R14) estimated by both Barnett et al. (2010) and Woodhouse et al. (2006) are tested here, as
148 are two records (R52,R53) for the Colorado River at Lee's Ferry (Meko et al. 2007;
149 Woodhouse et al. 2006). Finally, some of the Fig. 1 gauge stations measure flow for the same
150 rivers at various points in their watersheds, e.g., the Colorado
151 (R19,R22,R36,R38,R40,R51,R52), the Snake (R2-4) and the Green (R7, R12-14, R17)
152 Rivers.
153 Estimating pre-instrumental annual flow records from tree-ring data takes place in a general
154 framework (Fritts 1976; Meko et al 1995; also, see http://treeflow.info/study.html):
155
156 • Evaluating and conducting quality control of flow data from a gauge location whose
157 flow record is to be extended. If necessary, the data may be adjusted to correct for the
158 effects of diversions or non-climatic trends.
159 • Collecting and evaluating tree-ring data from multiple sites in or near the gauge's

watershed region. This includes site selection and tree coring, cross dating the cores from different trees, de-trending of ring width measurements to remove the 'age trend' effects of increasing trunk radius, and the removal of biological autocorrelation in ring widths. Finally, the resulting standardized ring width indices for numerous trees at a site are averaged to form a site dendrochronology.

- Forming a reconstruction model that estimates annual flow values from a set of predictor site chronologies during a calibration period common to both instrumental flow data and the site chronologies. These models are typically regression models, where the predictor variables can be actual site chronology time series (e.g. Woodhouse and Lukas 2006a; Watson et al. 2009; Gray et al. 2011), principal component (PC) series derived from the filtered ring width indices of individual trees (Meko 1997), PC series derived from site chronologies (Woodhouse et al 2006; Meko et al. 2001; Hidalgo et al. 2000), or PC series derived from flow reconstructions based on individual site chronologies (Meko et al. 2007; Hirschboeck and Meko 2008).
- Validating the reconstruction model using predictor variables and gauge data that were withheld from the regression training process.
- Evaluating the calibration and validation statistics. TreeFlow reconstructions report the portion of the annual flow variance explained by the regression model during the calibration period (R^2), the standard error of the estimate during the calibration period, a Reduction of Error (RE) statistic derived from the validation data, and the root square error of the regression during the validation period.

- Applying the model to the full length of the site chronology predictor data to generate reconstructed annual flow values in both the pre-instrumental and instrumental periods.

The R^2 and RE statistics for each of the reconstructions evaluated here can be found in Table 1. When multiple RE and R^2 are reported because different validation procedures are used (e.g., Margolis et al. 2011), or when multiple values are reported for different reconstruction periods (e.g., Meko et al. 2007; Hirschboeck and Meko 2008; Meko et al., 2001), Table 1 shows the lowest RE and R2 values. As defined by Cook et al. (1999, Appendix B) RE > 0.0 indicates predictive skill relative to a regression estimate defined by the calibration period's climatological mean. Table 1's RE scores range between 0.20 (R15) to 0.80 (R57). The median RE value is 0.59, and 46 of the RE values are greater than 0.50.

3 The Optimal Ranking Regime Method

The ORR method ranks a time series' data values, samples the rankings over running time windows of n_I years duration, then converts each sample of rankings into Mann-Whitney U and Z statistics (Mann and Whitney 1947). Although the U statistic for rankings within a sample window can be calculated based on the sample's size and rank sum (Mendenhall et al. 1990; Wilks 1995), the statistic is also equal to the total number of data values outside the sampling window that precede each sample value when all data values are arranged by rank (Hollander and Wolfe 1999). For a N-year reconstructed flow series divided into an n_I =21 year sample window and n_{II} = N-21 years outside the window, the highest possible U statistic

occurs when the sample contains the 21 highest ranked years [U = (N-21)*21]. A sample containing the 21 lowest ranked years produces the lowest U statistic [U=0*21]. Randomly sampled sets of 21 rankings produce U statistics that are normally distributed between those two extreme values, with values in the distribution's lower and upper tails indicating a high incidence of low and high ranked values in a sample. The U distribution's mean is equal to the average of the minimum and maximum U values, e.g.,

$$\mu_0 = 0.5\left[\left(0*21\right)+\left(21*\left(N-21\right)\right)\right] = 0.5*n_I*n_{II} \quad (1)$$

while the standard deviation can be estimated via Eq. 2 (Mendenhall et al. 1990),

$$\sigma_0 = \left(\left(n_I n_{II}*\left(n_I + n_{II} + 1\right)\right)/12\right)^{1/2} . \quad (2)$$

The Gaussian U statistics can be Z-normalized using these null parameters, with significantly low (high) Z values indicating a significant incidence of low (high) annual flow rankings relative to a null hypothesis that assumes random sampling (H_0).

$$Z_0 = \frac{U-\mu_0}{\sigma_0} \quad (3)$$

For a specific sample size, the Eq. 1 and 2 solutions for μ_0 and σ_0 assume that a sample's rankings are serially independent. However, in a multi-century reconstructed annual flow series, outcomes consistent with persistent 'red' variation are more likely in a sampled sequence of rankings. As a result, both null parameters were calculated here via Monte Carlo simulations consistent with a null hypothesis that allows for year-to-year persistence. This hypothesis (H_1) holds that the flow time series represents semi-random climate variation with inter-annual persistence, but is essentially stationary and trendless. The parameters of U null distributions consistent with H_1 were derived here via the following autoregressive (AR) modeling and Monte Carlo procedure:

i. As H_1 assumes that the time series is trendless, calculate AR(1), AR(2), and AR(3) regression coefficients from the autocorrelation values of the detrended reconstruction series. Then, select the AR model yielding the minimum Akaike Information Criteria score (Akaike, 1974).

ii. Use the AR model identified in step (i) to form AR red noise processes.

iii. Adjust the mean and variance of the red noise process resulting from step (ii) to agree with that of the data. Then, select red noise series with lengths equal to that of the time series being tested and rank those values.

iv. From the ranked noise processes resulting from step (iii) calculate appropriate null statistics, which in the preceding example would be U_I statistics derived from non-overlapping 21 element segments of each red noise series.

v. Repeat steps ii-iv until 50,000 independent null statistics are calculated, and determine the parameters of the resulting U_I null distribution.

Given the null distribution parameters derived from these Monte Carlo simulations (μ_1,σ_1), the Z statistics of rankings sampled from a reconstruction time series can be used to test H_1 .

$$Z_1 = \frac{U - \mu_1}{\sigma_1} \tag{4}$$

A sample's Z statistic is assigned based on which normalization, Z_0 or Z_1, produces the most conservative significance estimate. These assignments are determined mainly by the relative magnitudes of σ_0 and σ_1. Although the Monte Carlo generated μ_1 values agree closely with the corresponding Eq. 1 μ_0 values, σ_1 values generated using 6 to 100 year samples drawn from the rankings of the step (ii) red noise series were usually greater than the corresponding Eq. 2

249 σ_0 values. In those cases $|Z_1| < |Z_0|$, and Z statistics are calculated via Eq. 4. In instances
250 when the Monte Carlo generated σ_1 values are less than the σ_0 values, $|Z_1| > |Z_0|$, and
251 significance could be assigned to ranking samples that were consistent with white noise if the
252 Eq. 4 normalization was used. In those cases U statistics are normalized using Eq. 3. As a
253 result, the absolute value of the Eq. 3 Z_0 statistics serve as a ceiling limiting the magnitudes of
254 Z values, and helps to insure that significance is not assigned to ranking samples that were
255 consistent with essentially random white noise variation.
256 Figures 2a-e shows the ORR method applied to Meko et al.'s (2007) Colorado River at Lee's
257 Ferry (CRLF) flow reconstruction during 1500-2005. Figure 2a shows the annual flow values
258 and their 21-year running mean, while Fig. 2b shows the Z statistics for flow rankings
259 sampled over running 21-year windows. The horizontal lines in Fig. 2b mark the Z statistics'
260 negative and positive significance at two-sided 95%, and 99% confidence levels, and a dry
261 and wet shade scheme that marks negative and positive significance at both levels. Figure 2c's
262 dry and wet shade horizontal lines show the 21-year ranking regimes indicated as negatively
263 or positively significant at a 95% or better confidence level in Fig. 2b, superimposed on the
264 CRLF series. The vertical placement of those horizontal regime segments shows the ranking
265 regime's corresponding Z statistic, which is measured on the figure's right axis.
266 To apply the ORR procedure to an extended range of time scales, U and Z statistics were
267 calculated with moving sampling windows between 6 and 100 years in length. For every
268 sample size, running Z_0 and Z_1 statistics were calculated for each time series, and, as
269 described above, Z values were defined by the normalization that produced the smallest Z
270 magnitude. This normalization allows for significance testing of a specific sample size, as in
271 Fig. 2c, but also allows for comparing the significance of U statistics derived using different

272 sample sizes. After normalizing the running U statistics from each analysis, the positive and
273 negative Z statistics from all 95 tests that are significant at a 95% confidence level are
274 combined as in Fig. 2d. Those pooled statistics are then evaluated to identify ranking
275 sequences that are optimally significant over distinct, non-overlapping time windows (Fig.
276 2e). This process first sorts all the significant regime periods by the absolute value of the
277 period's Z statistic (|Z|) and then records the most significant statistic and its period. Then, the
278 next most significant |Z| value with a period that does not overlap with the most significant
279 ranking period is recorded. In the Fig. 2e CRLF series these leading statistics (Table 2)
280 occurred during a 1601-1621 wet regime (Z = 3.498) and two 6 year wet regimes with equal
281 rank sums and Z statistics during 1836-1841 and 1982-1987 (Z = 3.063). The ORR algorithm
282 iteratively proceeds by recording the next most significant |Z| statistic with a period that does
283 not overlap with all previously recorded periods, and continues until all the significant ranking
284 regimes identified by the 95 running tests have been tested. In the CRLF series the most
285 significant sequence of low flow years occurred during 1870-1904 (Z= -2.742). While the Z-
286 normalization process allows for comparing the significance of Z statistics derived using
287 varying sample sizes, it also makes it possible to rank the optimal ranking regimes found in a
288 reconstruction series. As a time series' ORR Z statistics can be interpreted as measures of
289 regime intensity, the most intense CRLF pluvial and drought periods in Fig. 2e occurred
290 during 1601-1621 and 1870-1904.
291 Figures 3a-d show the results of the ORR analysis when applied to the reconstructions of (a)
292 Columbia River flow at the Dalles, (b) Great Salt Lake level, (c) the Sacramento River Four
293 Rivers Index (Meko et al. 2001), and, (d), San Francisco Bay salinity. Because the method
294 defines non-overlapping high and low ranking regimes at two significance levels, compact

295 graphs can be formed showing the ORR results from multiple time series. Using Fig. 2b's
296 shading scheme for positive and negative significance, a time series' optimal ranking regimes
297 can be graphed on a single horizontal line referred to as a Z-line. The optimally significant
298 streamflow, lake level, and salinity regimes from Figs. 2e and 3a-d have been re-plotted as Z-
299 lines in Fig. 3e. By applying the ORR algorithm to all of Table 1's reconstructions, the
300 resulting Z-lines can be similarly arranged to show hydrological regime patterns over all of
301 Fig. 1's corresponding locations.
302
303 **4 ORR Analyses of Hydroclimate Reconstructions: 1500-2007**
304 Figure 4 shows the Z-lines for Table 1's 57 reconstructions during 1500-2007. The white
305 areas in that figure show each reconstruction's duration during that period, and each Z-line's
306 vertical coordinate is determined by the corresponding reconstruction number in Table 1 and
307 Fig. 1. These Z-lines will be referred to by their Table 1 reconstruction number, i.e., R1,
308 R2,…R57. The y-axis color backgrounds of Fig. 4's reconstruction numbers also follow Fig.
309 1's state color shading scheme. Thus R1-R14 are located in Fig. 1's light yellow states, R15-
310 R47 are located in Utah and Colorado, R48-R53 in New Mexico and Arizona, while R54-R57
311 are located in California. In the following the timing and duration of Fig. 4's drought and
312 pluvial regimes will be compared with those highlighted in previous work, particularly Fye
313 et al. (2003), Stahle and Dean (2011), and Cook et al. (2007), which were based on the
314 summer Palmer Drought Severity Index (PDSI) reconstructions of Cook et al.
315 (1996,1999,2004, 2007).
316
317

4.1 16th and 17th Centuries

Figure 4a outlines dry ORR periods beginning in the 1570's and ending on or before 1601. These dry periods coincide with the late 16th century 'megadrought' apparent in streamflow and PDSI reconstructions (Meko et al. 1995; Stahle et al. 2000,2007), which Meko et al. (1995) and Stahle et al. (2007) describe as occurring during 1579-1598 and 1559-1582 respectively. Stahle and Dean (2011) describe this period as " … the most severe sustained North American drought evident in the tree-ring record for the past 500 years". In the ORR analysis of the Fig. 2e CRLF reconstruction this drought's effects are apparent as a low flow regime during 1579-1592. However, as measured by that 14 year period's Z statistic (Table 2), that dry regime is the second most intense in the Meko et al. (2007) CRLF reconstruction during 1500-2005.

Following the late 16th century drought was a multi-decadal wet period during the early 17th century (Fig. 4b). This drought to pluvial transition is clearly seen in the Great Salt Lake level reconstruction (Fig. 3b, R15), and clearly significant wet regimes are also found in the upper Rio Grande (R50) and both CRLF reconstructions (R52, R53) during this time. Based on an analysis of gridded PDSI reconstructions, Fye et al. (2003) also note a western U.S. pluvial period during 1602-1622. The earliest onset year in Fig. 4b's optimally wet periods is 1601, while the latest termination year is 1622.

After 1621 dry periods re-appear in many proxy records that showed drought conditions during the late 16th century (Fig. 4c). In some instances these dry regimes are of longer duration and higher significance than the same reconstruction's previous dry periods in Fig. 4a, e.g., those in Fig. 4c's R19, R24, R32-R36, and R40 reconstructions. Figure 4c's multi-decadal drought pattern tends to be more consistent in the R2-R14 eastern Idaho and

341 Wyoming streamflow reconstructions. Fye et al. (2003) note drought conditions over this area
342 during 1624-1633, but the Fig. 4c low flow regimes are of generally longer duration.
343 In Fig. 4d brief drought periods are detected after many of the Fig. 4c dry regimes. However,
344 it is unclear whether these are two distinct drought events as some extended regimes span
345 both periods. The Woodhouse et al. (2006) CRLF reconstruction (R53) contains a 50 year dry
346 ORR period during 1622-1671 that is the longest and most significant low flow regime in that
347 record (Table 3). Dry regimes of similar duration and significance are found in the Colorado
348 River at Hot Sulphur Springs (R19), Big Thompson (R24), Blue River at Dillon (R34), and
349 Colorado River near Cisco (R40) reconstructions in Fig. 4c and d. The duration of Fig. 4d's
350 dry regimes coincides with the 1666-1671 Pueblo Drought period (Cook et al. 2007; Stahle
351 and Dean, 2011), which is also noted by Fye et al. (2003) as occurring during 1663-1672. The
352 earliest onset year of the Pueblo Drought regimes detected here is 1662, while the latest
353 termination year is 1672. After 1671 brief wet regimes, most ending in 1683 or before, are
354 found in many of the reconstructions (Fig. 4e).
355
356 **4.2 18th Century**
357
358 Compared to the 1575-1683 period in Fig. 4, 1700-1825 is marked by the relative absence of
359 consistent drought or pluvial patterns. One exception is Fig. 4f's pattern of dry periods evident
360 over the upper Colorado and upper Rio Grande watersheds (i.e., R36-R48, R50, R52, R53)
361 during the 1770's and early 1780's. Many of these ORR periods, including those in the two
362 CRLF reconstructions (R52, R53), coincide with the 1772-1782 time window attributed to
363 this drought by Fye et al. (2003). Figure 4f's drought periods immediately preceded the Año
364 del Hambre ("Year of Hunger") drought that affected northern Mexico and the Southern Great
365 Plains during 1785-1787 (Stahle and Dean, 2011). Although the 18th century appears to be

366 relatively free of extended drought or pluvial regimes over the Fig. 1 watershed regions, this
367 period may not have been generally drought-free over western North America. Before the
368 Año del Hambre period and the drought regimes of Fig. 4f, a series of indigenous rebellions
369 have been associated with drought conditions in northern Mexico during 1725-1742
370 (Brenneman, 2009).
371 Fresh water inflow to San Francisco Bay from the Sacramento-San Joaquin Delta has a
372 controlling influence on the bay's salinity levels (Stahle et al. 2001). In the mid-18th century
373 the California reconstructions (R54-R57) show a semi-consistent pattern of wet (dry)
374 streamflow regimes that coincide with fresh (salty) San Francisco Bay salinity (SFBNaCl)
375 regimes. During 1740-1747 high flow periods are found in the Feather River (R55) and
376 Sacramento-Four (R56) reconstructions, while a significant incidence of fresh, low-ranked,
377 SFBNaCl values (R57) are detected during 1738-1746 (Fig. 4g). In the 1770's these regimes
378 reverse sign, with low streamflow periods indicated in the Feather River and Sacramento-Four
379 records during 1776-1783, while a salty SFBNaCl regime is detected during 1775-1783 (Fig.
380 4h). Immediately after that period in Fig. 4h a fresh SFBNaCl regime occurs during 1784-
381 1792, while the Sacramento-Four and Feather River reconstructions show high flow periods
382 during that same time. Although the Salinas River at Paso Robles (R54) does not flow into
383 San Francisco Bay, it's Z-line also shows consistent periods of low and high flow with the
384 Feather River and Sacramento Four flow regimes in Figs. 4g and h.
385

386 **4.3 19th Century**

387 After 1825 pluvial conditions are widely apparent outside of California and the most northern
388 streamflow reconstructions (R1-R5), with the years 1836-1841 indicated as the most common
389 wet ORR period (Fig. 4i). Both Stahle and Dean (2011) and Fye et al (2003) consider this

390 pluvial to have occurred during 1825-1840, and the significant ranking regimes in Fig. 2d's
391 CRLF series during that time also indicates significant wet periods beginning in the late
392 1820's over the upper Colorado watershed. However, Fig. 4i's ORR results suggest that the
393 most significant concentrations of wet years occurred after 1835. This wet period was
394 followed by dry regimes in the early 1840's (Fig. 4j). Woodhouse et al. (2002) attribute this
395 drought to 1845-1856 based on an analysis of 60 tree-ring chronologies from the Rocky
396 Mountains, the Colorado Front Range, and the Great Plains. Stahle and Dean (2011) assign
397 this dry period to 1841-1865, and consider it the longest and most severe reconstructed
398 drought over the Great Plains and western North America during the 19th century. In Fig. 4i
399 the most common dry ORR periods occur during 1842-1847 and 1842-1848, and are generally
400 not highly significant, i.e., at a 99% confidence level. During this time, however, the
401 reconstructed flow for the Columbia River at the Dalles (R1, Fig. 3a) does show a highly
402 significant sequence (Z = -3.309) of low flow conditions during 1839-1852. After the low-
403 flow ORR periods of Fig. 4j, Fig. 4k outlines a consistent pattern of brief (6-8 year) wet
404 periods that, for the most part, begin after 1861 and end before 1871. The most common high
405 flow period is 1864-1869, which coincides closely with the 1867-1869 'Garden Myth' wet
406 period over the western U.S. described by Cook et al. (2007). Although Cook et al (2007)
407 note a second wet episode over the western U.S. during 1877–1879, that wetness was
408 not found in the reconstructed summer PDSI over the WY-UT-CO region (their Fig. 13).
409 A shift to wet conditions is also found in the reconstructed Columbia River flow during this
410 time (Fig. 3a), although, unlike Fig. 4j's dry periods, the 1860-1881 Columbia high flow
411 period is generally more significant (Z = 2.916) and spans both 'Garden Myth' periods.

412 After 1869 dry regimes, many of multi-decadal duration, are apparent over most of the R7-
413 R53 reconstructions (Fig. 4l). Between 1870 and the early 20th century Fye et al. (2003) note
414 separate southwestern U.S. drought periods during 1870-1883 and 1897-1904, while Stockton
415 and Jacoby (1976) note a single extended period of low flow in their CRLF reconstruction
416 during 1870-1894. The 1870-1904 low flow regime in the Meko et al. (2007) CRLF
417 reconstruction (R52) is the longest ORR of either sign in that record, and also it's most
418 significant ORR dry period (Z = -2.742) since 1500 (Table 2). However, a low flow period
419 during 1874-1883 in the Woodhouse et al. (2006) CRLF reconstruction (R53) has a shorter
420 duration and is only the third most significant dry regime during that time (Table 3). Other
421 reconstructions that show multi-decadal dry regimes significant at a 99% confidence level in
422 Fig. 4l include R18, R20-R22, R29, R31-R33, and R39.
423
424 **4.4 20th Century**
425
426 Figure 4m outlines early 20th century high flow conditions apparent in most of the
427 reconstructions apart from the California (R54-R57) and Columbia River flow (R1) records.
428 The most common beginning year in these wet periods is 1905, and most end on or before
429 1934. Wet periods in six reconstructions, however, persist into the 1940's and early 1950's
430 (R20, R22, R33, R36, R44, and R48). Fye et al. (2003) and Stahle and Dean (2011) define this
431 pluvial's duration as 1905-1917 and 1907-1916 respectively based on their analyses of
432 reconstructed summer PDSI. These high flow periods are most consistently and significantly
433 detected in gauge stations in Idaho and Wyoming (R2-R20), and in southern Colorado, New
434 Mexico, and Arizona (R44-R53), but are not as clearly apparent in the reconstructions for
435 upper Colorado and upper South Platte gauge stations in northern Colorado (R21-R52).

436 Despite the relative lack of significant wet regimes in the upper Colorado watershed in Fig.
437 4m, wet periods are detected in the Meko et al. (2007) CRLF reconstruction (R52) during
438 1905-1928 and in the Woodhouse et al. (2006) CRLF reconstruction (R53) during 1905-1932.
439 Stockton and Jacoby (1976) identified a Colorado River high flow period during 1906-1930,
440 and cited it as the longest and greatest period of anomalously high flow in their 1512-1961
441 CRLF reconstruction. However, the highest magnitude positive ORR Z statistic in both the
442 Meko et al. (Table 2) and Woodhouse et al. CRLF reconstructions (Table 3) occur during
443 1601-1621. Although the 1905-1928 and 1905-1932 wet periods are the longest in those
444 reconstructions, the corresponding Z statistics rank 3rd (Table 2) and 4th (Table 3)
445 respectively.
446 Figure 4 shows little evidence of the effects of the 1930's drought, which were mainly
447 centered over the Great Plains in the analyses of Shubert et al. (2004) and Mauget (2003a). In
448 the analysis of Fye et al. (2003) drought conditions during 1929-1940 also extend into parts of
449 the Columbia River watershed. A 1922-1941 low flow regime in the Columbia River
450 reconstruction (R1, Fig. 3a) overlaps with the Fye et al. (2003) drought period, but also
451 precedes it. Unlike the drought of the 1930's, the 1950's drought had strong precipitation
452 effects over Colorado and New Mexico during 1950-1956 (Mauget 2003a). But apart from
453 early 1950's low flow regimes in R29-R31, R44, and R50, there is also no widespread
454 evidence of that drought's effects in the Fig. 4 reconstructions.
455 In Fig. 4n a pattern of high flow regimes beginning in the mid-1960's and ending in the mid-
456 1980's is evident in the Idaho and Wyoming reconstructions (R2-R5, R7-R11). One of Fig.
457 4's most consistent patterns of pluvial regimes is found in R12-R53 in the mid 1980's (Fig.
458 4o). Woodhouse and Lukas (2006a) refer to a period of unusually abundant moisture in

459 Colorado during 1982-1999, but in Fig. 4o's flow reconstructions the most common wet ORR
460 period is 1982-1987. Although most of the Fig. 4 reconstructions end during or before the
461 1999-2004 drought period in the western U.S. (Piechota et al., 2004; Cook et al., 2007), R2-
462 R4 and R49 show low flow ORR periods during 2000-2005 and 2000-2006.
463
464 **4.5 Centennial Scale Variation**
465 Apart from the four California reconstructions (R54-R57), Fig. 4's dominant variability
466 patterns are evident as alternating drought-pluvial regimes during the late 16^{th} and 17^{th}
467 centuries (Fig. 4a-e) and also during the 19^{th} and early 20^{th} centuries (Fig. 4i-m). But between
468 those two periods, with the exception of low flow conditions in R29-R53 during the 1770's
469 (Fig. 4f), many of the reconstructions are more consistent with red noise during 1680-1835.
470 An example of this lack of significant IMD variation is seen in the R23-R25 reconstructions,
471 which have no ranking regimes significant at a 95% confidence level during 1719-1830 (Fig.
472 4p). These periods of active and dormant hydroclimate variability are more evident when the
473 number of Z-lines that are in significant ($|Z| \geq 1.96$) drought and pluvial regimes are counted
474 for each year of 1500-2000. In Fig. 4q these counts are expressed as percentages of the total
475 number of R1-R53 Z-lines that are defined in a particular year, which is determined by the
476 duration of the reconstruction records. As few lines extend past the year 2000, the Fig. 4q
477 percentages are not calculated during 2001-2007. During 1580-1680 and 1835-1930 relatively
478 high percentages (> 40%) of the R1-R53 Z-lines experienced alternating wet and dry IMD
479 regimes. However, between those two periods, years in which more than 40% of the
480 reconstructions are in a drought or pluvial ORR period are relatively rare. As a result, the Fig.
481 4 ORR analyses generally show two active centennial scale periods marked by alternating

482 IMD wet and dry regimes, separated by a period during the 18th and early 19th century with
483 relatively little IMD regime variation. Similar centennial scale variability in the Cook et al.
484 (1999) summer PDSI reconstructions was noted over western U.S. grid locations by Hidalgo
485 (2004). That analysis calculated the percentage of the PDSI total power spectral density in
486 bidecadal (8-32 year) and pentadecadel (32-64 year) frequency bands during three periods:
487 1525-1650, 1700-1825, and 1850-1975. Pentadecadal PDSI variation was dominant during the
488 1525-1650 and 1850-1975 periods over grid locations in the interior west, but virtually absent
489 during 1700-1825 (Hidalgo 2004; his Figs. 3d,e,f). Conversely, higher frequency bidecadal
490 PDSI variation was relatively strong during 1700-1825, but less apparent during the 1525-
491 1650 and 1850-1975 periods (Hidalgo 2004; his Figs. 3a,b,c).
492 Decadal to multi-decadal variation in U.S. hydroclimate has been associated with similarly
493 persistent regimes in North Pacific and North Atlantic sea-surface temperature; i.e., those
494 associated with the Pacific Decadal Oscillation (PDO) and the Atlantic Multidecadal
495 Oscillation (AMO), and with regimes in the El Niño-Southern Oscillation (ENSO) mechanism
496 (see review in McCabe and Wolock 2013). Oceanic forcing is generally thought to play a
497 central role in sustaining persistent climate regimes (Schubert et al. 2004,2008; Cook et al.
498 2007; Solomon et al. 2010; Hoerling et al. 2011). Over the interior western U.S. the combined
499 influence of the AMO and PDO are considered to be particularly important (Gray et al. 2003;
500 Hidalgo 2004; McCabe et al. 2004, 2007). As a result, Fig. 4q's patterns of relatively active
501 and inactive periods of IMD variation lead to questions as to whether similar variation is
502 evident in PDO, AMO, and ENSO reconstructions. A commonly studied influence over the
503 western U.S is the PDO, which has been associated with pre-instrumental precipitation
504 regimes in PDO reconstructions derived from tree-ring chronologies (Gedalof and Smith,

505 2001; Biondi et al. 2001; MacDonald and Case, 2005). However, as Mantua and Hare (2002)
506 and D'Arrigo and Wilson (2006) note, the variation in these PDO reconstructions are
507 frequently inconsistent. This lack of consensus was also found here in the ORR analyses of
508 four PDO reconstructions (Appendix A). Moreover, the Z-lines for those reconstructions,
509 and for reconstructions of the AMO and a unified ENSO proxy series, show no obvious
510 similarity to Fig. 4q's centennial scale pattern of active and inactive IMD variation (Fig. A2).
511 As a result, even though those consistent patterns of drought and pluvial activity suggest an
512 oceanic influence, the ORR analyses of Appendix A's reconstructed North Pacific and North
513 Atlantic climate indices show no clear evidence of that influence.
514
515 **5 Summary and Discussion**
516
517 The Optimal Ranking Regime (ORR) method was used to identify intra- to multi-decadal
518 (IMD) variation in reconstructed records of western U.S. streamflow, the level of the Great
519 Salt Lake (Fig. 3b), and San Francisco Bay salinity levels (Fig. 3d) during 1500-2007. The
520 ORR algorithm, which is described in Section 3 and demonstrated in Figs. 2a-e, detects the
521 most significant sequences of low and high ranked values in a time series relative to a null
522 hypothesis that holds that the series consists of trendless red noise. As these optimal ranking
523 sequences are defined over non-overlapping 6-100 year time windows, the associated periods
524 of low and high rankings in a reconstruction series, and their significance at 95% and 99%
525 confidence levels, can be displayed on graphically concise horizontal traces referred to as Z-
526 lines (Figs. 3e and 4).
527 As described in Section 3, Mann-Whitney U statistics for samples of rankings are normally
528 distributed, with values in a U distribution's lower and upper tails indicating a sample with a
529 high incidence of low or high rankings. In the ORR procedure U statistics calculated over

530 running sampling windows are normalized into Z statistics (Eqs. 3,4), which allows for
531 determining the significance of each running sample. Because these running analyses are
532 repeated with varying sample sizes, this normalization also allows for comparing the
533 significance of Z statistics derived using each sample size. The optimal ranking regimes
534 detected by this 'brute-force' algorithm are the most significant ranking sequences in all the
535 running analyses that occur over non-overlapping time windows (e.g., Fig. 2e). Because each
536 ORR's Z statistic is a measure of the regime's concentration of extreme low or high rankings,
537 those statistics can also be used to rank the intensity of a reconstruction's leading drought and
538 pluvial regimes. However, because Eq. 4's μ_1 and σ_1 null parameters are calculated via a
539 Monte Carlo (MC) process that uses random number generators, the magnitudes of ORR Z
540 statistics can vary slightly between successive applications of the algorithm. This is primarily
541 due to variation in the σ_1 parameter, which can lead to slight variation in the magnitudes of Z
542 statistics in separate runs of the algorithm.

543 In Tables 2 and 3 the five wettest and driest flow regime periods were defined for the Meko et
544 al. (2007) and Woodhouse et al. (2006) reconstructions of Colorado River at Lee's Ferry
545 (CRLF) flow based on the Z statistics of their optimal ranking regimes. In addition, the
546 longest high and low flow periods were highlighted. When those ORR analyses are repeated
547 twice with different MC simulations the leading regime's Z magnitudes vary slightly from the
548 Table 2 and 3 values, but the ordering of the wettest and driest regimes, and the longest
549 duration periods, are unchanged (Appendix B). As a result, those rankings, and the relative
550 intensity of reconstructed low and high CRLF flow regimes, appear insensitive to variation in
551 the σ_1 parameter from different MC simulations. Although Stockton and Jacoby (1976)
552 identified 1906-1930 as the leading period of high flow in their 450 year CRLF

553 reconstruction, the most significant sequence of rankings found here in the Meko et al. and
554 Woodhouse et al. CRLF reconstructions occurred during 1601-1621. In other cases the
555 intensity of ORR drought periods over the interior western U.S. detected here seems
556 inconsistent with previous analyses based on reconstructed summer PDSI. Although Goodrich
557 (2007) and Stahle and Dean (2011) cite the late 16th century drought (Fig. 4a) as the most
558 severe North American drought evident in the tree-ring record during the past 500 years, the
559 drought regimes in the Z-lines outlined in Figs. 4c and d during the 17th century appear
560 stronger in both duration and intensity over the WY-UT-CO region. In the Woodhouse et al.
561 CRLF reconstruction the driest ORR period occurred during 1622-1671 (Table 3). Stahle and
562 Dean (2011) cite 1841-1865 as the most severe drought over the Great Plains and western
563 North America during the 19th century based on reconstructed PDSI analyses, yet that period
564 shows relatively weak evidence of dry regimes in Fig. 4j. Based on the magnitudes of ORR Z
565 statistics, a more intense 19th century drought over the upper Colorado watershed is indicated
566 here during 1870-1904 in Fig. 4l, which is also the Meko et al. CRLF reconstruction's driest
567 period (Fig. 2e, Table 2).

568 For the most part, the ORR analyses conducted here were of streamflow reconstructions from
569 the TreeFlow web data resource (http:/treeflow.info). As described in Section 4.4 and
570 summarized in Fig. 4q, a common pattern in these analyses is that of IMD cycles of drought
571 and pluvial regimes during the late 16th and 17th centuries (Fig. 4a-e), a period with relatively
572 little variability during the 18th century, and the reappearance of alternating drought and
573 pluvial periods during the 19th and early 20th centuries (Fig. 4i-m). Although studies
574 summarizing reconstructed U.S. hydroclimate tend to emphasize extended drought (e.g.,
575 Meko et al. 1995; Woodhouse and Overpeck 1998; Cook et al. 1999; Cole et al. 2002; Cook et

576 al. 2007), less attention is generally paid to pluvial periods (Woodhouse et al. 2005).
577 However, over the interior western U.S. the results here indicate two centennial-scale periods
578 marked by drought-pluvial cycles, separated by an 18th century period that was, in a climatic
579 sense, comparatively quiet.
580 But although Fig. 4's individual ORR analyses of reconstructed streamflow show consistent
581 regime patterns, the Table 1 streamflow reconstructions may not be completely independent.
582 As many of these reconstructions were done by individual groups (e.g. Barnett et al. 2010,
583 Wise 2010) and are from adjacent watersheds, some may reflect flow variability estimated
584 from overlapping sets of dendrochronologies. As noted in Section 2, a number of the Table 1
585 reconstructions are for flow for the same rivers at various points in their watershed. Also,
586 because these reconstructions are mostly representative of the upper Colorado watershed and
587 the WY-UT-CO region (Table 1, Fig. 1), Fig. 4's overall regime pattern may not represent
588 variability over the broader western U.S. Whether this is the case might be resolved in the
589 future via an ORR analysis of the more spatially continuous Cook et al. (2007) PDSI
590 reconstructions.
591 However, over the upper Colorado region, the consistency of Fig. 4's reconstructed flow
592 regime patterns does suggest a real signal in centennial-scale hydroclimate. Given the current
593 conception of the role of oceanic mechanisms in driving the IMD hydrology of the upper
594 Colorado River basin (McCabe et al. 2007) and the western U.S. in general (Redmond and
595 Koch, 1991; Cayan et al. 1998; Dai 2013), this leads to questions as to whether those
596 mechanisms may also experience centennial-scale periods of active and dormant variability.
597 As described in Section 4.5, such variation has been noted by Hidalgo (2004) in reconstructed
598 summer PDSI over the western U.S. The leading modes of Hidalgo's (2004) rotated principal

599 component analysis of the Cook et al. (1999) summer PDSI reconstructions show common
600 features with the Biondi et al. (2001) PDO reconstruction and the AMO reconstruction of
601 Gray et al. (2004). As a result, he concluded that extended droughts over the interior western
602 U.S. may be a consequence of combined PDO and AMO effects. However, the ORR analyses
603 of four independently derived PDO reconstructions in Figs. A1c-f, which includes the Biondi
604 et al. (2001) reconstruction (PDO-B), show no common regime features. Appendix A's
605 ORR analyses of a unified ENSO proxy series and of North Atlantic sea-surface temperature
606 anomalies also show no evidence of regime patterns similar to that of Fig. 4q. However, this
607 may not indicate that Fig. 4q's centennial scale signal in reconstructed streamflow occurred
608 independently of oceanic variability. The lack of common regime patterns in the ORR
609 analyses of the Appendix A PDO reconstructions suggests that Pacific decadal variation
610 during the pre-instrumental period is, at this time, essentially unknown. However, the ORR
611 method might be used to indirectly detect that variability. The current approach of inferring
612 the state of the pre-instrumental PDO typically involves comparing tree ring or coral
613 chronologies with observed PDO (Gedalof and Smith, 2001; Biondi et al. 2001; MacDonald
614 and Case, 2005) or Northern Pacific Index (D'Arrigo et al. 2005) data to develop regression
615 models. An alternative approach might involve applying ORR analysis to networks of
616 streamflow or temperature reconstructions around the Pacific basin, e.g., TreeFlow data
617 counterparts in Asia or South America. Consistent regime patterns from ORR analyses of
618 dense networks of Asian and North American reconstructions, or from a transect of
619 reconstructions spanning the western coasts or North and South America (e.g., Villalba et al.
620 2001, 2011), might indirectly show a common low frequency Pacific influence.
621 The ORR method may be a useful option for evaluating IMD variability in reconstructed

622 climate records. Because it is based on the analysis of data rankings, it is insensitive to the
623 influence of data outliers and to how data is distributed. The method does not involve the use
624 of subjectively selected thresholds or filters to detect low frequency variation, but instead uses
625 an exhaustive and relatively objective algorithm to find the most significant ranking regimes
626 occurring over a range of IMD time scales. The graphic approach to displaying Z-lines
627 demonstrated here in Figs. 3e and 4 can help to identify consistent regime patterns in
628 numerous reconstructions, and to corroborate variability in reconstructions produced by
629 different investigators using different methods. These features may make the method
630 particularly useful in evaluating the extensive data sets being generated in millennial-scale
631 regional temperature reconstructions (PAGES 2k Consortium 2013). The Z-line diagrams may
632 also highlight climate regimes that appear as outliers relative to those in other data records.
633 Examples in Fig. 4 of such possible behavior are the 99 year low flow regime in the Wind
634 River (R5) reconstruction during 1561-1659, and the 64 year dry regime in the Canadian
635 River Z-line (R48) during 1845-1908. However, some features of the ORR method may also
636 lead users to consider more traditional methods such as runs analysis (Dracup 1980). Because
637 of it's use of Monte Carlo simulated null parameters, attempts at ranking the intensity and
638 duration of optimal regime periods in a reconstruction series, e.g., as in the CRLF
639 reconstructions in Tables 2 and 3, may require repeated applications of the algorithm to verify
640 rank ordering. It is also possible that runs analysis may be more useful to water managers who
641 need estimates of the probability of a drought or pluvial period of a specified duration (e.g.,
642 Biondi 2002, 2005).
643

Appendix A: ORR Analyses of Pacific and North Atlantic Climate Indices

As in Fig. 2e, Figs. A1a-f show the results of ORR analyses of six reconstructions of North Atlantic and Pacific climate variability during 1500-1998. Table A1 summarizes the first and last years of the reconstructions, their calibration periods where applicable, and references. As these reconstructions follow variation in sea-surface temperature anomalies (SSTA), optimal ranking regimes significant at 95% and 99% confidence levels are marked in Figs. A1 and A2 with the warm shade-cool shade significance scheme shown at the top of Fig. A1. Thus in the analyses of North Atlantic sea-surface temperatures anomalies (NATSSTA) and a Unified ENSO Proxy (UEP) series red (blue) shades indicate anomalously warm (cool) SSTA regimes over the North Atlantic and equatorial Pacific. In the Pacific Decadal Oscillation (PDO) analyses red (blue) shades mark warm (cool) SSTA periods in the Gulf of Alaska and along the western coast of North America.

Figure A1a shows IMD regimes of cold and warm NATSSTA conditions derived from the reconstructions of Gray et al. (2004). Figure A1b shows the ORR analysis of the UEP series of McGregor et al. (2010). The UEP series is the leading principal component of a PCA of 10 reconstructions that reflect ENSO variation, and is considered to represent those series' common ENSO signal during 1650-1977. As the low-passed UEP series shows IMD variability similar to that of the Pacific Decadal Oscillation (PDO) during the 20th century, McGregor et al. (2010) also consider it as a potential PDO proxy.

Figures A1c-f shows the ORR analyses of four PDO reconstructions. The PDO-B (c) series is the reconstruction of Biondi et al. (2001), which was based on Southern California and Northern Baja California tree-ring records and reconstructs Nov.-Mar. PDO variation between 1661 and 1991. The PDO-D (d) series is D'Arrigo and Wilson's (2006)

668 reconstruction of boreal spring (March-May) PDO during 1565-1988 based on Asian and
669 Siberian tree-ring records. The PDO-M (e) reconstruction of MacDonald and Case (2005)
670 was based on California and Alberta tree-ring records. The PDO-M values reconstruct
671 annual (Jan.-Dec.) PDO during 993-1996, but only the 1500-1996 values were tested in the
672 Fig. A1e ORR analysis. The PDO-S (f) series is Shen et al.'s (2006) reconstruction of
673 annual PDO during 1470-1998 based on a summer drought/flood index derived from
674 Chinese historical documents. Like the PDO-M analysis, only the 1500-1998 PDO-S values
675 were subjected to ORR analysis in Fig. A1f.
676 Figure A2 shows the Z-lines for the NATSSTA, UEP, and PDO-B,D,M, and S ORR
677 analyses, and compares those regime periods with the variation in R1-R53 streamflow
678 regimes plotted in Fig. 4q. Cool PDO regimes are evident in all four PDO reconstructions
679 and the UEP reconstruction during the 1940's to mid-1970's (Fig. A2a) , which generally
680 coincides with the 1947-1976 cool phase period defined by Mantua et al. (1997). Although
681 the UEP, PDO-B and PDO-M reconstructions also show warm PDO regimes during 1905-
682 1915, 1906-1923 and 1906-1928 (Fig. A2b), those periods precede Mantua et al.'s 1925-
683 1946 warm phase PDO period. However, the regimes detected in the PDO-S reconstruction
684 during the 20th century (Fig. A2c) more closely follow Mantua et al.'s PDO phase periods,
685 with warm phase conditions during 1926-1942 and cool phase conditions during 1948-1977.
686 After the mid 1970's, the warm phase regime in the PDO-S reconstruction during 1978-
687 1998 also closely coincides with Mantua et al.'s warm phase period after 1976. But
688 although there is some agreement between the UEP and PDO reconstructions during the
689 instrumental calibration periods (Table A1), there is virtually no agreement in the pre-
690 instrumental period. In the one instance where the Pacific reconstructions show clearly

691 concurrent regimes before 1900 those regimes are of opposite sign, i.e., the PDO-M and
692 PDO-D reconstructions roughly coincident cold and warm phase regimes during 1619-1718
693 and 1626-1703 (Fig. A1d). As a result, the PDO and UEP indices show essentially no
694 common behavior in the pre-instrumental period, and when compared with Fig. 4q, no
695 evidence of centennial scale periods of active and inactive variability.
696 In Fig. A2 during the 20th century the optimal ranking regimes of the NATSSTA
697 reconstruction include a 1926-1961 warm regime, which nearly coincides with the 1931-
698 1960 warm phase period defined by Sutton and Hodson (2005). However, Sutton and
699 Hodson (2005) also defined cool North Atlantic SSTA periods during 1905-1925 and
700 1965-1990, which the ORR procedure did not detect in the NATSSTA series at a 95%
701 confidence level. The ORR analysis detected multi-decadal cool regimes in the
702 reconstructed NATSSTA series during 1597-1625 and 1801-1847 and a warm regime
703 during 1656-1696, but, like the Pacific analyses of Figs. A1b-f, show no patterns of
704 centennial variability similar to that of the reconstructed streamflow described in Section 4.4
705 and graphed in Figs. 4q and A2.
706

Table A1

	Reconstruction Period	Calibration Period	Reference
NATSSTA	1567-1990	1922-1990	Gray et al. (2004)
UEP	1650-1977	NA	McGregor et al. (2010)
PDO-B	1661-1991	1962-1991/1925-1954	Biondi et al. (2001)
PDO-D	1565-1988	1917-1960	D'Arrigo and Wilson (2006)
PDO-M	993-1996	1940-1996	MacDonald and Case (2005)
PDO-S	1470-1998	1925-1998	Shen et al. (2006)

Table A1. Reconstruction periods, calibration periods, and references for the North Atlantic SSTA (NATSSTA), Unified ENSO Proxy (UEP) and PDO-B,D,M, and S reconstructions of Figs. A1a-f.

Appendix B

Table B1

|Z| Rank	Period	Duration (Years)	Z	Period	Duration (Years)	Z
1	1601-1621	21	3.497	1870-1904	**35**	-2.727
2	1982-1987/1836-1841	6	3.068	1579-1592	14	-2.421
3	1905-1928	**24**	2.806	1772-1782	11	-2.344
4	1672-1683	12	2.541	1663-1671	9	-2.223
5	1741-1747	7	1.966	1622-1632	11	-2.203
	Wet Periods			Dry Periods		

Table B1: As in Table 2 with an alternate random number generator seed.

Table B2

|Z| Rank	Period	Duration (Years)	Z	Period	Duration (Years)	Z
1	1601-1621	21	3.498	1870-1904	**35**	-2.742
2	1982-1987/1836-1841	6	3.064	1579-1592	14	-2.424
3	1905-1928	**24**	2.797	1772-1782	11	-2.331
4	1672-1683	12	2.523	1663-1671	9	-2.208
5	1741-1747	7	1.965	1622-1632	11	-2.191
	Wet Periods			Dry Periods		

Table B2: As in Tables 2 and B1 with an alternate random number generator seed.

Table B3

|Z| Rank	Period	Duration	Z	Period	Duration	Z
1	1601-1621	21	3.491	1622-1671	**50**	-2.679
2	1836-1841	6	3.250	1772-1782	11	-2.441
3	1982-1987	6	3.055	1874-1883	10	-2.196
4	1905-1932	**28**	2.658	1842-1847	6	-1.991
5	1687-1702	16	2.498	1528-1533	6	-1.913
	Wet Periods			Dry Periods		

Table B3: As in Table 3 with an alternate random number generator seed.

Table B4

|Z| Rank	Period	Duration	Z	Period	Duration	Z
1	1601-1621	21	3.498	1622-1671	**50**	-2.677
2	1836-1841	6	3.251	1772-1782	11	-2.449
3	1982-1987	6	3.056	1874-1883	10	-2.192
4	1905-1932	**28**	2.654	1842-1847	6	-1.992
5	1687-1702	16	2.493	1528-1533	6	-1.914
	Wet Periods			Dry Periods		

Table B4: As in Tables 3 and B3 with an alternate random number generator seed.

Program Access and Acknowledgements

The calc_orr.c program and an associated shell script are available in the supplementary material. Thanks to Matthew Becker and Justin DeRose of the Wasatch Dendroclimatology Research Group for the Weber River flow and Great Salt Lake Level reconstruction data, and to Z'ev Gedalof for the Columbia River flow reconstruction. All figures were produced using Generic Mapping Tools (Wessel and Smith, 1995). The U.S. Department of Agriculture is an equal opportunity provider and employer.

References

Akaike, H.: A new look at the statistical model identification, IEEE T Automat Contr, ac-19, 716-723, 1974.

Barnett, F., Gray, S., and Tootle, G.: Upper Green River Basin (United States) streamflow reconstructions, J Hydrol Eng, 15, 567-579, 2010.

Bekker, M. F., DeRose, R.J., Buckley, B.M., Kjelgren, R.K., and Gill, N.S. : A 576-year Weber River streamflow reconstruction from tree rings for water resource risk assessment in the Wasatch Front, Utah, J Am Water Resour As, 50, 1338-1348, 2014.

Biondi, F., Gershunov, A., and Cayan, D. R.: North Pacific decadal climate variability since 1661, J Climate, 14, 5-10, 2001.

Biondi, F., Kozubowski, T. J., and Panorska, A. K.: Stochastic modeling of regime shifts, Climate Res, 23, 23-30, 2002.

Biondi, F., Kozubowski, T. J., and Panorska, A. K.: A new model for quantifying climate episodes, Int J Climatol, 25, 1253-1264, 2005.

800 Box, G. E. P., and Tiao, G. C.: Intervention analysis with applications to economic and
801 environmental problems, J Am Stat Assoc, 70, 70-79, 1975.
802 Brenneman, D.: Climate of rebellion: The relationship between climate variability and
803 indigenous uprisings in mid-eighteenth-century Sonora, PhD Dissertation, Univ. of
804 Arizona Anthropology Dept., University of Arizona, Tucson, AZ, 2004.
805 Cayan, D. R., Dettinger, M. D., Diaz, H. F., and Graham, N. E.: Decadal variability of
806 precipitation over western North America, J Climate, 11, 3148-3166, 1998.
807 Cole J.E., Overpeck, J.T., and Cook, E.R.: Multiyear La Niña events and persistent
808 drought in the contiguous United States, Geophys Res Lett, 29, 25-1 - 25-4 , 2002.
809 Cook, E. R., Meko, D. M., Stahle, D.W. and Cleaveland, M.K.: Tree Rings, Environment,
810 and Humanity, Eds., Radio- carbon, 155–169.: Tree-ring reconstructions of past
811 drought across the conterminous United States: Tests of a regression method and
812 calibration/verification results. In: Tree Rings, Environment, and Humanity, J. S. Dean,
813 D. M. Meko, T. W. Swetnam (Ed.), Department of Geosciences, University of Arizona
814 ,Radiocarbon, Tucson, 1996.
815 Cook, E. R., Meko, D. M., Stahle, D. W., and Cleaveland, M. K.: Drought Reconstructions
816 for the Continental United States, J Climate, 12, 1145-1162, 1999.
817 Cook, E. R., Woodhouse, C. A., Eakin, C. M., Meko, D. M., and Stahle, D. W.: Long-term
818 aridity changes in the western United States, Science, 306, 1015-1018, 2004.
819 Cook, E. R., Seager, R., Cane, M. A., and Stahle, D. W.: North American drought:
820 Reconstructions, causes, and consequences, Earth-Science Reviews, 81, 93-134, 2007.
821 Cordero, E., Kessomkiat, W., Abatzoglou, J., and Mauget, S.: The identification of distinct
822 patterns in California temperature trends, Climatic Change, 108, 357-382, 2011.

823 Creasman, P. P., Bannister, B., Towner, R. H., Dean, J. S., and Leavitt, S. W.: Reflections
824 on the foundation, persistence, and growth of the Laboratory of Tree-Ring Research,
825 circa 1930–1960, Tree-Ring Research, 68, 81-89, 2012.
826 D'Arrigo, R. and Wilson, R.: On the Asian expression of the PDO, Int J Climatol, 26,
827 1607-1617, 2006.
828 D'Arrigo, R., Wilson, R., Deser, C., Wiles, G., Cook, E., Villalba, R., Tudhope, A., Cole, J.,
829 and Linsley, B.: Tropical–North Pacific climate linkages over the past four centuries, J
830 Climate, 18, 5253-5265, 2005.
831 Dai, A.: The influence of the inter-decadal Pacific oscillation on US precipitation during
832 1923–2010, Climate Dynamics, 41, 633-646, 2013.
833 DeRose, R. J., Wang, S.-Y., Buckley, B. M., and Bekker, M. F.: Tree-ring reconstruction of
834 the level of Great Salt Lake, USA, The Holocene, 24, 805-813, 2014.
835 Dracup, J. A., Lee, K. S., and Paulson, E.G. : On the Definition of Droughts, Water Resour
836 Res, 16, 297-302, 1980.
837 Fritts, H. C.: Tree Rings and Climate, Academic Press, London, 1976.
838 Fye, F. K., Stahle, D. W., and Cook, E. R.: Paleoclimatic Analogs to Twentieth-Century
839 Moisture Regimes Across the United States, B Am Meteorol Soc, 84, 901-909, 2003.
840 Gedalof, Z., and Smith, D.J.: Interdecadal climate variability and regime-scale shifts in
841 Pacific North America, Geophys Res Lett, 28, 1515-1518, 2001.
842 Gedalof, Z., Peterson, D.L., and Mantua N.: Columbia River Flow and Drought since
843 1750, J Am Water Resour As, 2004. 1579-1592, 2004.
844 Goodrich, G. B.: Multidecadal Climate Variability and Drought in the United States,
845 Geography Compass, 1, 713-738, 2007.

Gray, S.T., Betancourt, J.L., Fastie, C.L., and Jackson, S.T.: Patterns and sources of multidecadal oscillations in drought-sensitive tree-ring records from the central and southern Rocky Mountains, Geophys Res Lett, 30, DOI: 10.1029/2002GL016154, 2003.

Gray, S.T., Graumlich, L.J., Betancourt, J.L., and Pederson, G.T.: A tree-ring based reconstruction of the Atlantic Multidecadal Oscillation since 1567 A.D., Geophys Res Lett, 31, L12205, doi:10.1029/2004GL019932, 2004.

Gray, S. T., Lukas, J. J., and Woodhouse, C. A.: Millennial-Length Records of Streamflow From Three Major Upper Colorado River Tributaries, J Am Water Resour As, 47, 702-712, 2011.

Griffin, R. D.: A 600-Year Streamflow History in the Salinas Valley Reconstructed from Blue Oak Tree Rings, M.A. Thesis, University of Arkansas, Fayetteville, 67 pp., 2007.

Hidalgo, H. G.: Climate precursors of multidecadal drought variability in the western United States, Water Resour Res, 40, W12504, 2004.

Hidalgo, H. G., Piechota, T. C., and Dracup, J. A.: Alternative principal components regression procedures for dendrohydrologic reconstructions, Water Resour Res, 36, 3241-3249, 2000.

Hirschboeck, K. K. and Meko., D. M.: The Current Drought In Context: A Tree-Ring Based Evaluation of Water Supply Variability for the Salt-Verde River Basin Final Report, University of Arizona Laboratory of Tree-Ring Research & The Salt River Project, Tucson, AZ, 29 pp., 2008.

Hoerling, M., Hurrell, J., Kumar, A., Terray, L., Eischeid, J., Pegion, P., Zhang, T., Quan, X., and Xu, T.: On North American Decadal Climate for 2011–20, J Climate, 24, 4519-4528, 2011.

869 Hollander, M. and Wolfe, D. A.: Nonparameteric Statistical Methods, Wiley and Sons,
870 Hoboken, 1999.
871 Hundley, N.: Water and the West: The Colorado River Compact and the Politics of
872 Water in the American West, University of California Press, Oakland, CA, 2009.
873 MacDonald, G. M. and Case, R. A.: Variations in the Pacific Decadal Oscillation over the
874 past millennium, Geophys Res Lett, 32, L08703, doi: 10.1029/2005GL022478, 2005.
875 MacDonnell, L. J., Getches, D. H., and Hugenberg, W. C.: The Law of the Colorado River:
876 Coping with Severe Sustained Drought, J Am Water Resour As , 31, 825-836, 1995.
877 Mann, H. B. and Whitney, D. R.: On a Test of Whether One of Two Random Variables is
878 Stochastically Larger than the Other, Ann Math Stat, 18, 50-60, 1947.
879 Mantua, N. J., Hare, S. R., Zhang, Y., Wallace, J. M., and Francis, R. C.: A Pacific
880 Interdecadal Climate Oscillation with Impacts on Salmon Production, B Am Meteorol
881 Soc, 78, 1069-1079, 1997.
882 Mantua, N. J. and Hare, S. R.: The Pacific Decadal Oscillation, J Oceanogr, 58, 35-44,
883 2002.
884 Margolis, E. Q., Meko, D. M., and Touchan, R.: A tree-ring reconstruction of streamflow
885 in the Santa Fe River, New Mexico, J Hydrol, 397, 118-127, 2011.
886 Masiokas, M. H., Villalba, R., Christie, D. A., Betman, E., Luckman, B. H., Le Quesne, C.,
887 Prieto, M. R., and Mauget, S.: Snowpack variations since AD 1150 in the Andes of Chile
888 and Argentina (30°–37°S) inferred from rainfall, tree-ring and documentary records, J
889 Geophys Res-Atmos, 117, D05112, doi: 10.1029/2011JD016748, 2012.
890 Mauget, S. A.: Intra- to Multidecadal Climate Variability over the Continental United
891 States: 1932–99, J Climate, 16, 2215-2231, 2003a.

892 Mauget, S. A.: Multidecadal Regime Shifts in U.S. Streamflow, Precipitation, and
893 Temperature at the End of the Twentieth Century, J Climate, 16, 3905-3916, 2003b.
894 Mauget, S. A.: Low Frequency Streamflow Regimes over the Central United States:
895 1939–1998, Climatic Change, 63, 121-144, 2004.
896 Mauget, S. A., and E. C. Cordero. : Optimal Ranking Regime Analysis of Intra- to Multi-
897 Decadal U.S. Climate Variability. Part I: Temperature. J Climate, 27,9006-9026, 2014a.
898 Mauget, S., and E. C. Cordero.: Optimal Ranking Regime Analysis of Intra- to Multi-
899 decadal U.S. Climate Variability. Part II: Precipitation and Streamflow, J Climate. 27,
900 9027-9049, 2014b.
901 McCabe, G. J. and Wolock, D. M.: Variability Common to Global Sea Surface
902 Temperatures and Runoff in the Conterminous United States, J Hydrometeorol, 15,
903 714-725, 2013.
904 McCabe, G. J., Palecki, M.A., and J. Betancourt, J.L.: Pacific and Atlantic Ocean influences
905 on multidecadal drought frequency in the United States, P Natl Acad Sci USA, 101,
906 4136–4141, 2004.
907 McCabe, G. J., Betancourt, J. L., and Hidalgo, H. G.: Associations of Decadal to
908 Multidecadal Sea-Surface Temperature Variability with Upper Colorado River Flow, J
909 Am Water Resour As, 43, 183-192, 2007.
910 McGregor, S., Timmermann, A., Timm, O.: A unified proxy for ENSO and PDO variability
911 since 1650, Clim Past, 1-17, 2010.
912 Meko, D.: Dendroclimatic Reconstruction with Time Varying Predictor Subsets of Tree
913 Indices, J Climate, 10, 687-696, 1997.

914 Meko, D., Stockton, C. W., and Boggess, W. R.: The tree ring record of severe sustained
915 drought., J Am Water Resour As, 31, 789-801, 1995.
916 Meko, D. M., Therrell, M. D., Baisan, C. H., and Hughes, M. K.: Sacramento river flow
917 reconstructed to A.D. 869 from tree rings, J Am Water Resour As, 37, 1029-1039, 2001.
918 Meko, D. M., Woodhouse, C. A., Baisan, C. A., Knight, T., Lukas, J. J., Hughes, M. K., and
919 Salzer, M. W.: Medieval drought in the upper Colorado River Basin, Geophys Res Lett,
920 34, L10705, doi:10.1029/2007GL029988, 2007.
921 Meko, D. M. and Woodhouse, C.W.: Application of Streamflow Reconstruction to Water
922 Resources Management. In: Dendroclimatology: Progress and Prospects, Hughes, M. K.,
923 , T.W. Swetnam and H.F. Diaz (Ed.), Developments in Paleoenvironmental Research,
924 Springer, New York, 231-261, 2011.
925 Mendenhall, W., Wackerly, D.D. and Sheaffer, R.L.: Mathematical Statistics with
926 Applications. PWS-Kent, Boston, 1990.
927 Nash, S. E.: Time, Trees, and Prehistory: Tree Ring Dating and the Development of
928 North American Archaeology 1914-1950, The University of Utah Press, Salt Lake City,
929 1999.
930 Pagano, T., Pasteris, P., Dettinger, M., Cayan, D., and Redmond, K.: Water year 2004:
931 Western water managers feel the heat, Eos, Transactions American Geophysical Union,
932 85, 385-393, 2004.
933 PAGES 2k Consortium.: Continental-scale temperature variability during the past two
934 millennia, Nat Geosci, 6, 339-346, 2013.
935 Piechota, T., Timilsena, J., Tootle, G. and Hidalgo, H: The western U.S.. drought: How bad
936 is it? Eos, Transactions, American Geophysical Union, 85, 301-308, 2004

937 Redmond, K. T. and Koch, R. W.: Surface Climate and Streamflow Variability in the
938 Western United States and Their Relationship to Large-Scale Circulation Indices, Water
939 Resour Res, 27, 2381-2399, 1991.
940 Rice, J. L., Woodhouse, C.A., and Lukas, J.J.: Science and Decision Making: Water
941 Management and Tree-Ring Data in the Western United States, J Am Water Resour As,
942 45, 1248-1259, 2009.
943 Salas J.D, Delleur, J.W., Yevjevich, V.M., and Lane, W.L. : Applied Modelling of Hydrologic
944 Time Series, Water Resources Publication, Littleton, CO, 1980.
945 Shen, C., Wang, W., Gong, W., Hao, Z.: A Pacific Decadal Oscillation record since 1470 AD
946 reconstructed from proxy data of summer rainfall over eastern China, Geophys Res
947 Lett, 33, L03702, doi:10.1029/2005GL024804, 2006.
948 Schubert, S. D., Suarez, M. J., Pegion, P. J., Koster, R. D., and Bacmeister, J. T.: Causes of
949 Long-Term Drought in the U.S. Great Plains, J Climate, 17, 485-503, 2004.
950 Schubert, S. D., Suarez, M. J., Pegion, P. J., Koster, R. D., and Bacmeister, J. T.: Potential
951 Predictability of Long-Term Drought and Pluvial Conditions in the U.S. Great Plains, J
952 Climate, 21, 802-816, 2008.
953 Solomon, A., Goddard, L., Kumar, A., Carton, J., Deser, C., Fukumori, I., Greene, A. M.,
954 Hegerl, G., Kirtman, B., Kushnir, Y., Newman, M., Smith, D., Vimont, D., Delworth, T.,
955 Meehl, G. A., and Stockdale, T.: Distinguishing the Roles of Natural and
956 Anthropogenically Forced Decadal Climate Variability, B Am Meteorol Soc, 92, 141-
957 156, 2010.
958 Stahle, D. W. and Dean, J. S.: North American Tree Rings, Climate Extremes, and Social
959 Disasters. In: Dendroclimatology: Progress and Prospects, M.K. Hughes, T. W. S., and

960 H.F. Diaz (Ed.), Developments in Paleoenvironmental Research, Springer, New York,
961 297-327, 2011.
962 Stahle, D. W., Cook, E. R., Cleaveland, M. K., Therrell, M. D., Meko, D. M., Grissino-Mayer,
963 H. D., Watson, E., and Luckman, B. H.: Tree-ring Data Document 16th Century
964 Megadrought Over North America, Eos, Transactions, American Geophysical Union, 81,
965 121-125, 2000.
966 Stahle, D. W., Therrell, M. D., Cleaveland, M. K., Cayan, D. R., Dettinger, M. D., and
967 Knowles, N.: Ancient blue oaks reveal human impact on San Francisco Bay salinity, Eos,
968 Transactions American Geophysical Union, 82, 141-145, 2001.
969 Stahle, D.W. Fye, F.K, Cook, E.R., Griffin, R. D.: Tree-ring reconstructed megadroughts
970 over North America since A.D. 1300, Climatic Change, 83, 133-149, 2007.
971 Stockton, C. W., and Jacoby, G. C.: Long-term surface-water supply and streamflow
972 trends in the Upper Colorado River Basin, Lake Powell., Natl. Sci. Found. (Ed.),
973 Arlington, VA, 1976.
974 Sutton, R. T. and Hodson, D. L. R.: Atlantic Ocean Forcing of North American and
975 European Summer Climate, Science, 309, 115-118, 2005.
976 Villalba, R., Luckman, B. H., Bosinsegna, J., D'Arrigo, R. D., Lara, A., Villenueva-Diaz, J.,
977 Masiokas, M., Argollo, J., Soliz, C., LeQuesne, C., Stahle, D. W., Roig, F., Aravena, J. C.,
978 Hughes, M. K., Wiles, G., Jacoby, G., Hartsough, P., Wilson, R. J. S., Watson, E., Cook, E. R.,
979 Serano-Paredes, J., Therrell, M., Cleaveland, M., Morales, M. S., Graham, N. E., Moya, J.,
980 Pacajes, J., Massacchesi, G., Biondi, F., Urrutia, R., and Pastur, G. M.: Dendroclimatology
981 from Regional to Continental Scales: Understandimg Regional Processes to
982 Reconstruct Large Scale Climate Variations Across the Western Americas. In:

983 Dendroclimatology: Progress and Prospects, M.K. Hughes, Swetnam, T. W., and Diaz, H.
984 F. (Eds.), Springer, New York, 175-227, 2011.
985 Villalba, R., R. D'Arrigo, E. Cook, G. Wiles, and G. Jacoby: Decadal-scale climatic
986 variability along the extratropical western coast of the Americas: Evidence from tree-
987 ring records. In: Inter-Hemispheric Climate Linkages, Markgraf, V. (Ed.), Academic
988 Press, San Diego, 155-172, 2001.
989 Watson, T. A., Anthony, B.F., Gray, S. T., and Tootle, G. A.: Reconstructed Streamflows
990 for the Headwaters of the Wind River, Wyoming, United States, J Am Water Resour As,
991 45, 224-236, 2009.
992 Wessel, P. and Smith, W. H. F.: New version of the generic mapping tools, Eos,
993 Transactions American Geophysical Union, 76, 329-329, 1995.
994 Wilks, D. S.: Statistical Methods in the Atmospheric Sciences, Academic Press, San Diego ,
995 1995.
996 Wise, E. K.: Tree ring record of streamflow and drought in the upper Snake River,
997 Water Resour Res, 46, W11529, doi: 10.1029/2010WR009282, 2010.
998 Woodhouse, C. A. and Lukas, J. J.: Multi-Century Tree-Ring Reconstructions of Colorado
999 Streamflow for Water Resource Planning, Climatic Change, 78, 293-315, 2006a.
1000 Woodhouse, C.A. and Lukas, J. J.: Streamflow Reconstructions for Boulder Creek, South
1001 Boulder Creek, and the Colorado River., City of Boulder and Hydrosphere Resource
1002 Consultants, Boulder, CO, 2006b.
1003 Woodhouse, C.A. and Lukas., J. J.: Tree-ring reconstruction of Clear Creek annual
1004 streamflow, 1566-2002, Report to City of Westminster, Westminster, CO, 2006c.

1005 Woodhouse, C. A. and Overpeck, J. T.: 2000 Years of Drought Variability in the Central
1006 United States, B Am Meteorol Soc, 79, 2693-2714, 1998.
1007 Woodhouse, C. A., Lukas, J. J., and Brown, P. M.: Drought in the Western Great Plains,
1008 1845–56, B Am Meteorol Soc, 83, 1485-1493, 2002.
1009 Woodhouse, C.A., Kunkel, K.E., Easterling, D.R., and Cook, E.R.: The twentieth-century
1010 pluvial in the western United States, Geophys Res Lett, 32, L07701, doi:
1011 10.1029/2005GL022413, 2005.
1012 Woodhouse, C. A., Gray, S. T., and Meko, D. M.: Updated streamflow reconstructions for
1013 the Upper Colorado River Basin, Water Resour Res, 42, W05415,
1014 doi:10.1029/2005WR004455, 2006.
1015
1016
1017

Table 1

R#	Location	Begin Year	End Year	R2	RE	Citation
1	Columbia R. at Dalles OR	1750	1987	0.25	0.24	Gedalof et al. 2004
2	Snake R. near Heise, ID	1591	2005	0.63	0.59	Wise 2010
3	Snake R. near Irwin, ID	1591	2005	0.66	0.59	Wise 2010
4	Snake R. near Moran, WY	1591	2005	0.56	0.52	Wise 2010
5	Wind R. near Dubois, WY	1560	1992	0.45	0.36	Watson et al. 2009
6	Little Popo Agie R. near Lander, WY	1560	1999	0.58	0.5	Watson et al. 2009
7	Green R. near Daniel, WY	1615	1999	0.44	0.38	Barnett et al.2010
8	Pine Creek above Fremont Lake, WY	1615	1999	0.53	0.48	Barnett et al.2010
9	East Fork R. near Big Sandy, WY	1615	1999	0.58	0.51	Barnett et al.2010
10	Hams Fork near Frontier, WY	1615	1999	0.48	0.43	Barnett et al.2010
11	Fontanelle Creek near Fontanelle, WY	1615	1999	0.48	0.39	Barnett et al.2010
12	Green R. below Fontanelle Reservoir, WY	1615	1999	0.59	0.52	Barnett et al.2010
13	Green R. near Green River, WY	1525	1997	0.48	0.38	Woodhouse et al. 2006
14	Green R. near Green River, WY	1615	1999	0.6	0.54	Barnett et al.2010
15	Great Salt Lake Level Reconstruction	1429	2005	0.5	0.2	DeRose et al. 2014
16	Weber R. near Oakley, Utah	1429	2004	0.49	0.29	Bekker et al. 2014
17	Green River near Greendale, UT	1615	1999	0.65	0.58	Barnett et al.2010
18	Yampa River near Maybell, CO	1000	2002	0.6	0.56	Gray et al. 2011
19	Colorado R. at Hot Sulphur Springs, CO	1566	2002	0.7	0.67	Woodhouse and Lukas 2006b
20	Fraser R. at Granby, CO	1383	1999	0.73	0.69	Woodhouse and Lukas 2006a
21	Willow Creek Reservoir Inflow, CO	1383	1999	0.73	0.67	Woodhouse and Lukas 2006a
22	Colorado R. near Granby, CO	1383	1999	0.67	0.59	Woodhouse and Lukas 2006a
23	Cache la Poudre R. at Canyon Mouth, CO	1615	1999	0.64	0.56	Woodhouse and Lukas 2006a
24	Big Thompson R. at Mouth of Canyon, CO	1569	1999	0.72	0.65	Woodhouse and Lukas 2006a
25	St Vrain R. at Lyons, CO	1571	1999	0.65	0.61	Woodhouse and Lukas 2006a
26	Boulder Creek near Orodell, CO	1566	2002	0.64	0.6	Woodhouse and Lukas 2006b
27	S. Boulder Creek near Eldorado Springs, CO	1566	2002	0.69	0.65	Woodhouse and Lukas 2006b
28	Clear Creek near Golden, CO	1566	2002	0.7	0.66	Woodhouse and Lukas 2006c
29	N. Fork of South Platte R. at South Platte, CO	1685	1987	0.67	0.61	Woodhouse and Lukas 2006a
30	South Platte R. at South Platte, CO	1634	2002	0.76	0.71	Woodhouse and Lukas 2006a
31	South Platte R. below Cheesman Lake, CO	1685	1987	0.63	0.58	Woodhouse and Lukas 2006a
32	Fraser R. at Winter Park, CO	1437	2002	0.67	0.62	Woodhouse and Lukas 2006a
33	Williams Fork R. near Leal, CO	1437	2002	0.67	0.62	Woodhouse and Lukas 2006a
34	Blue R. at Dillon, CO	1437	2002	0.63	0.59	Woodhouse and Lukas 2006a
35	Blue R. above Green Mountain Reservoir, CO	1539	1999	0.76	0.7	Woodhouse and Lukas 2006a
36	Colorado River near Kremmling, CO	1440	2002	0.7	0.64	**/upco/coloradokremmling.html
37	Roaring Fork River at Glenwood Springs, CO	1402	1999	0.69	0.63	**/upco/roaringfork.html

Table 1 (Cont.)

R#	Location	Begin Year	End Year	R2	RE	Citation
38	Colorado River at Glenwood Springs, CO	1525	1997	0.72	0.65	Woodhouse et al. 2006
39	White River near Watson, UT	1000	2002	0.61	0.58	Gray et al. 2011
40	Colorado River near Cisco, UT	1569	1997	0.77	0.73	Woodhouse et al. 2006
41	Gunnison River near Grand Junction, CO	1569	1997	0.77	0.73	Woodhouse et al. 2006
42	Gunnison River at Crystal Reservoir, CO	1569	1997	0.69	0.64	Woodhouse et al. 2006
43	Arkansas River at Canon City, CO	1685	1987	0.63	0.58	**/ark/arkansascanoncity.html
44	Saguache Creek near Saguache, CO	1520	2000	0.7	0.63	**/riogr/saguache.html
45	Rio Grande near Del Norte, CO	1508	2002	0.71	0.69	**/riogr/riograndedelnorte.html
46	Conejos River near Mogote, CO	1508	2002	0.67	0.63	**/riogr/conejos.html
47	Animas River at Durango, CO	1470	2002	0.82	0.8	**/upco/animas.html
48	Canadian R. near Sanchez, NM	1604	1997	0.61	0.51	**/ark/canadian.html
49	Rio Grande at Otowi Bridge, NM	1450	2002	0.74	0.72	**/riogr/riograndeotowinrcs.html
50	Santa Fe River near Santa Fe, NM	1592	2007	0.6	0.54	Margolis et al. 2011
51	Colorado River at Lees Ferry, AZ	762	2005	0.57	0.54	Meko et al. 2007
52	Colorado River at Lees Ferry, AZ	1490	1997	0.81	0.76	Woodhouse et al. 2006
53	Sum of Salt-Verde-Tonto waterways, AZ	1330	2005	0.49	0.45	Hirschboeck and Meko 2008
54	Salinas R. at Paso Robles, CA	1409	2003	0.73	0.68	Griffin 2007
55	Sacramento River - Four Rivers Index	901	1977	0.62	0.55	Meko 2001
56	Feather River inflow to Lake Oroville, CA	901	1977	0.61	0.54	Meko 2001
57	San Francisco Bay Salinity	1604	1997	0.82	0.8	Stahle et al. 2001

Table 1. Reconstruction number, location, beginning year, ending year, calibration period R^2, validation period reduction of error (RE), and citations or URLs (** = http://treeflow.info) for the reconstructions evaluated here.

Table 2

|Z| Rank	Period	Duration	Z	Period	Duration	Z
1	1601-1621	21	3.498	1870-1904	**35**	-2.742
2	1982-1987/1836-1841	6	3.063	1579-1592	14	-2.419
3	1905-1928	**24**	2.804	1772-1782	11	-2.332
4	1672-1683	12	2.530	1663-1671	9	-2.209
5	1741-1747	7	1.966	1622-1632	11	-2.192
	Wet Periods			Dry Periods		

Table 2 Periods, durations, and Mann Whitney Z statistics of the five wettest and driest ranking regimes in the ORR analysis of Meko et al.'s (2007) reconstruction of Colorado River flow at Lee's Ferry annual flow during 1500-2005. Bold duration numbers mark the longest wet and dry regime period.

Table 3

|Z| Rank	Period	Duration	Z	Period	Duration	Z
1	1601-1621	21	3.496	1622-1671	**50**	-2.695
2	1836-1841	6	3.230	1772-1782	11	-2.441
3	1982-1987	6	3.036	1874-1883	10	-2.171
4	1905-1932	**28**	2.647	1842-1847	6	-1.980
5	1687-1702	16	2.486	1528-1533	6	-1.902
	Wet Periods			Dry Periods		

Table 3 Periods, durations, and Mann Whitney Z statistics of the five wettest and driest ranking regimes in the ORR analysis of Woodhouse et al.'s (2006) reconstruction of Colorado River flow at Lee's Ferry annual flow during 1500-1997. Bold duration numbers mark the longest wet and dry regime periods.

Table A1

	Reconstruction Period	Calibration Period	Reference
NATSSTA	1567-1990	1922-1990	Gray et al. (2004)
UEP	1650-1977	NA	McGregor et al. (2010)
PDO-B	1661-1991	1962-1991/1925-1954	Biondi et al. (2001)
PDO-D	1565-1988	1917-1960	D'Arrigo and Wilson (2006)
PDO-M	993-1996	1940-1996	MacDonald and Case (2005)
PDO-S	1470-1998	1925-1998	Shen et al. (2006)

Table A1. Reconstruction periods, calibration periods, and references for the North Atlantic SSTA (NATSSTA), Unified ENSO Proxy (UEP) and PDO-B,D,M, and S reconstructions of Figs. A1a-f.

Figure Captions

Figure 1: Locations of the USGS gauge stations associated with the Table 1 flow reconstructions and the locations of San Francisco Bay and the Great Salt Lake.

Figure 2: a) Time series of Colorado River at Lee's Ferry reconstructed water year total natural flow (CRLF) during 1500-2005. b) Mann-Whitney Z statistics of ranked reconstructed flow values sampled over running 21 year time windows. Horizontal lines indicate two-sided 95% (Z= ±1.96) and 99% (Z = ±2.575) confidence intervals. c) As in (a) with horizontal extent of colored bars showing significant 21 year low and high flow ranking regimes as indicated in (b). Vertical placement of bars show corresponding Z values as marked by right axis. Color scheme on left axis shows positive and negative significance at 95%, and 99% confidence levels. d) As in (c) with significant low and high flow ranking regimes indicated by running Mann-Whitney Z analyses with 6,7,…,100 year sampling windows. e) The optimally significant low and high flow ranking regimes in (d) occurring over non-overlapping time windows.

Figure 3. a) As in Fig. 2e for the reconstructed flow of the Columbia River at The Dalles during 1750-1987. b) As in Fig. 2e for the reconstructed level of the Great Salt Lake during 1500-2005. c) As in Fig. 2e for the reconstructed Sacramento River - Four Rivers Index during 1500-1977. d) As in Fig. 2e for reconstructed San Francisco Bay salinity during 1604-1997. c) The optimal ranking regimes in Figs. 2e and 3a-d plotted as Z-lines. The significance shading scheme for Z statistics is as shown at the top.

1172 Figure 4. Z-lines for the optimal ranking regimes found in each of the Table 1
1173 reconstructions. The vertical axis marks the corresponding reconstruction number as found
1174 in Table 1. The vertical axis' yellow, cyan, violet, and green shaded regions mark Z-lines
1175 from reconstructions in the similarly shaded states in Fig. 1. Positive and negative
1176 significance at 95%, and 99% confidence levels is marked by the shading scheme at the top
1177 of Fig. 3. The a-p black frames outline regime features discussed in the text. q) The
1178 percentage of R1-R57 Z-lines that indicate significant drought or pluvial conditions ($|Z| \geq$
1179 1.96) during 1500-2000. Green traces indicate the percentage of lines in a pluvial regime,
1180 and orange traces show the percentage of lines in a drought regime during each year.
1181
1182 Figure A1. a) Optimal ranking regime analysis of the North Atlantic SSTA reconstruction of
1183 Gray et al. (2004). b) As in (a) for the Unified ENSO Proxy of McGregor et al. (2010). c)
1184 As in (a) for the PDO reconstruction of Biondi et al. (2001). d) As in (a) for the PDO
1185 reconstruction of D'Arrigo and Wilson (2006). e) As in (a) for the PDO reconstruction of
1186 MacDonald and Case (2005). f) As in (a) for the PDO reconstruction of Shen et al. (2006).
1187
1188 Figure A2. The optimal ranking regimes in Figs. A1e-f plotted as Z-lines. The significance
1189 shading scheme for Z statistics is as shown at the top of Fig. A1. The a-d black frames
1190 outline regime features discussed in the Appendix A text. The lower figure reproduces Fig.
1191 4q, which shows the percentage of Fig. 4's R1-R53 Z-lines that indicate significant drought
1192 or pluvial conditions ($|Z| \geq 1.96$) during 1500-2000. Green traces indicate the percentage of
1193 lines in a pluvial regime, and orange traces show the percentage of lines in a drought
1194 regime during each year.

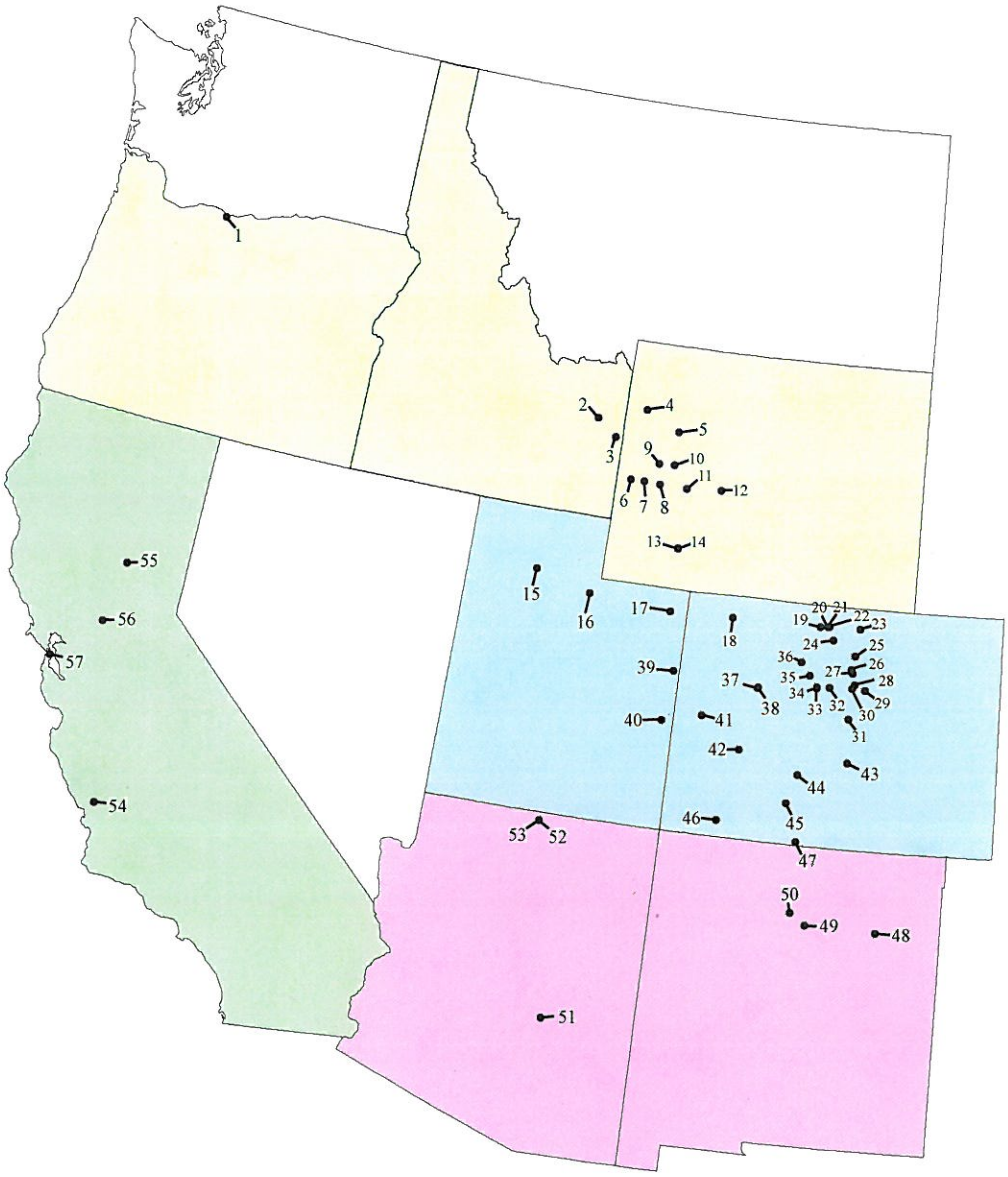

Figure 1: Locations of the USGS gauge stations associated with the Table 1 flow reconstructions and the locations of San Francisco Bay and the Great Salt Lake.

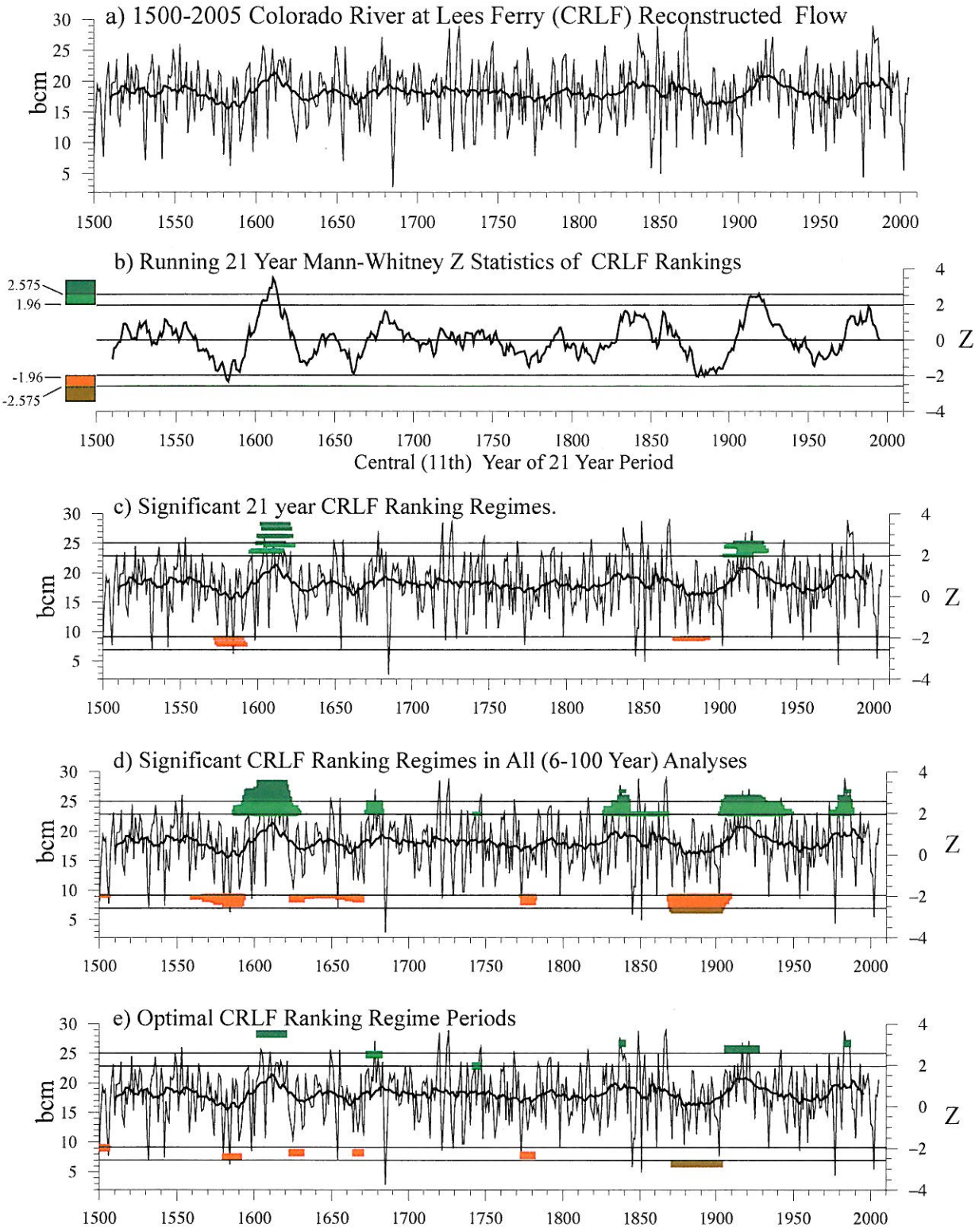

Figure 2: a) Time series of Colorado River at Lee's Ferry reconstructed water year total natural flow (CRLF) during 1500-2005. b) Mann-Whitney Z statistics of ranked reconstructed flow values sampled over running 21 year time windows. Horizontal lines indicate two-sided 95% (Z= ±1.96) and 99% (Z = ±2.575) confidence intervals. c) As in (a) with horizontal extent of colored bars showing significant 21 year low and high flow ranking regimes as indicated in (b). Vertical placement of bars show corresponding Z values as marked by right axis. Color scheme on left axis shows positive and negative significance at 95%, and 99% confidence levels. d) As in (c) with significant low and high flow ranking regimes indicated by running Mann-Whitney Z analyses with 6,7,...,100 year sampling windows. e) The optimally significant low and high flow ranking regimes in (d) occurring over non-overlapping time windows.

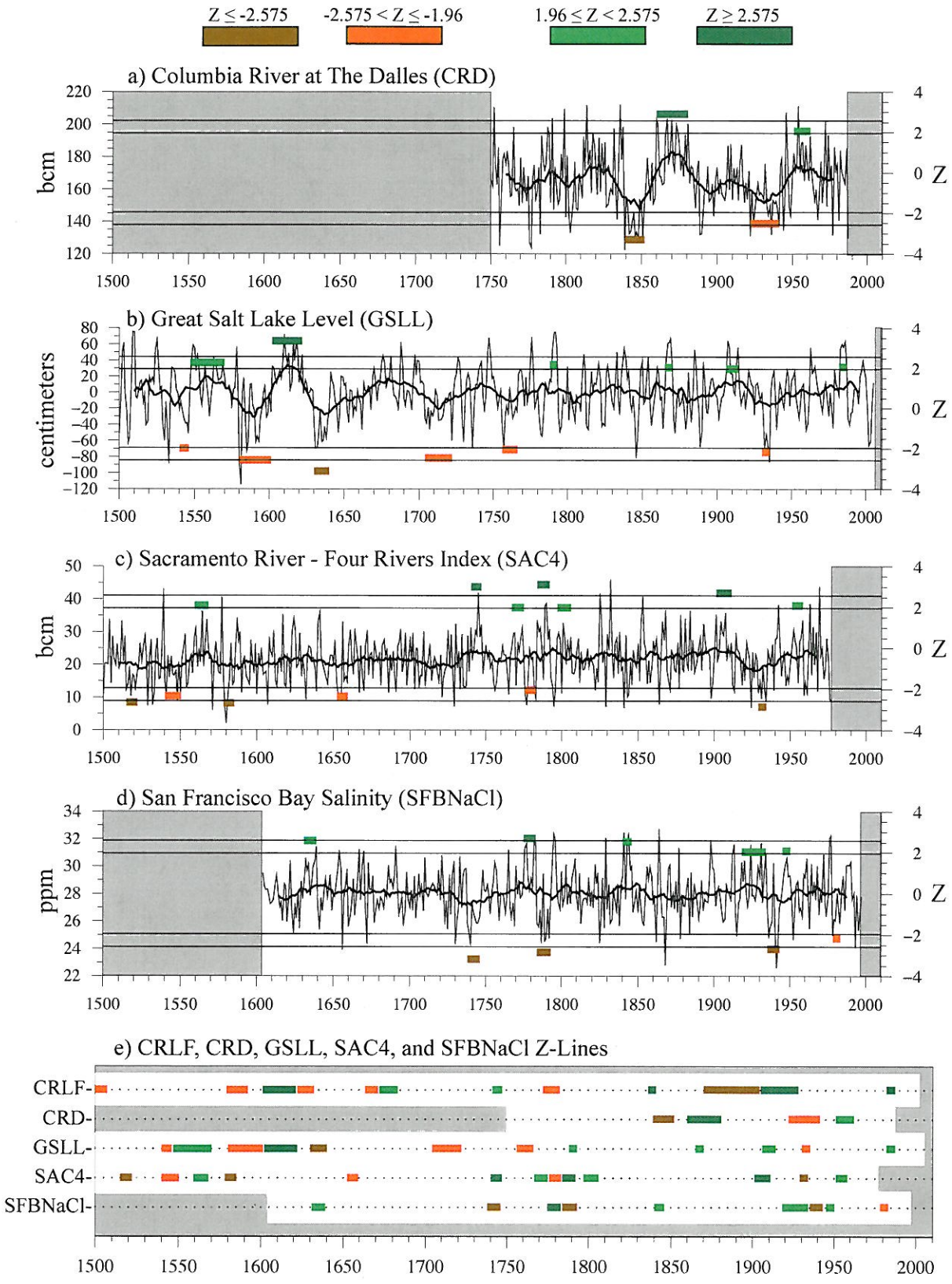

Figure 3. a) As in Fig. 2e for the reconstructed flow of the Columbia River at The Dalles during 1750-1987. b) As in Fig. 2e for the reconstructed level of the Great Salt Lake during 1500-2005. c) As in Fig. 2e for the reconstructed Sacramento River - Four Rivers Index during 1500-1977. d) As in Fig. 2e for reconstructed San Francisco Bay salinity during 1604-1997. c) The optimal ranking regimes in Figs. 2e and 3a-d plotted as Z-lines. The significance shading scheme for Z statistics is as shown at the top.

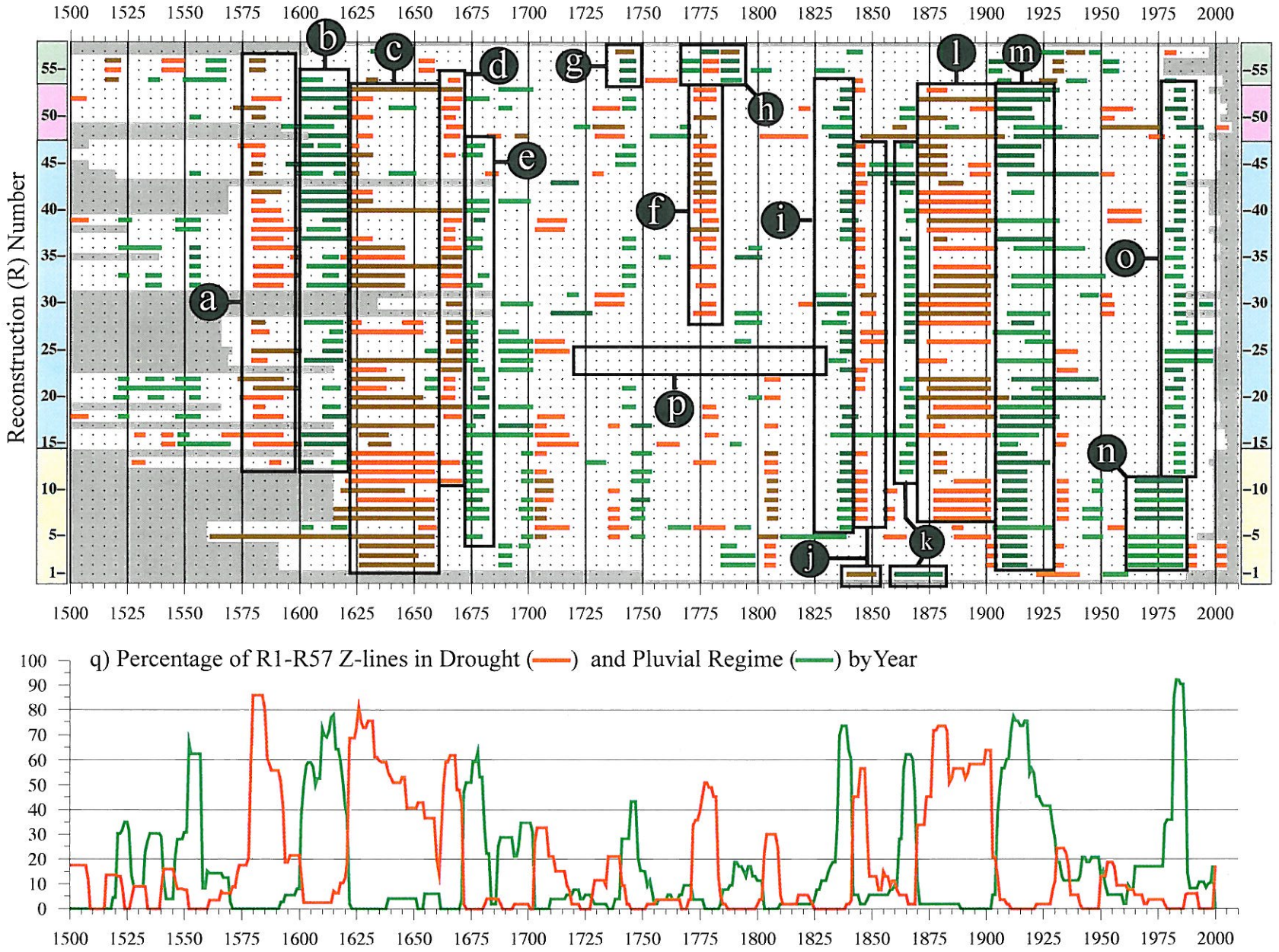

Figure 4. Z-lines for the optimal ranking regimes found in each of the Table 1 reconstructions. The vertical axis marks the corresponding reconstruction number as found in Table 1. The vertical axis' yellow, cyan, violet, and green shaded regions mark Z-lines from reconstructions in the similarly shaded states in Fig. 1. Positive and negative significance at 95%, and 99% confidence levels is marked by the shading scheme at the top of Fig. 3. The a-p black frames outline regime features discussed in the text. q) The percentage of R1-R57 Z-lines that indicate significant drought or pluvial conditions ($|Z| \geq 1.96$) during 1500-2000. Green traces indicate the percentage of lines in a pluvial regime, and orange traces show the percentage of lines in a drought regime during each year.

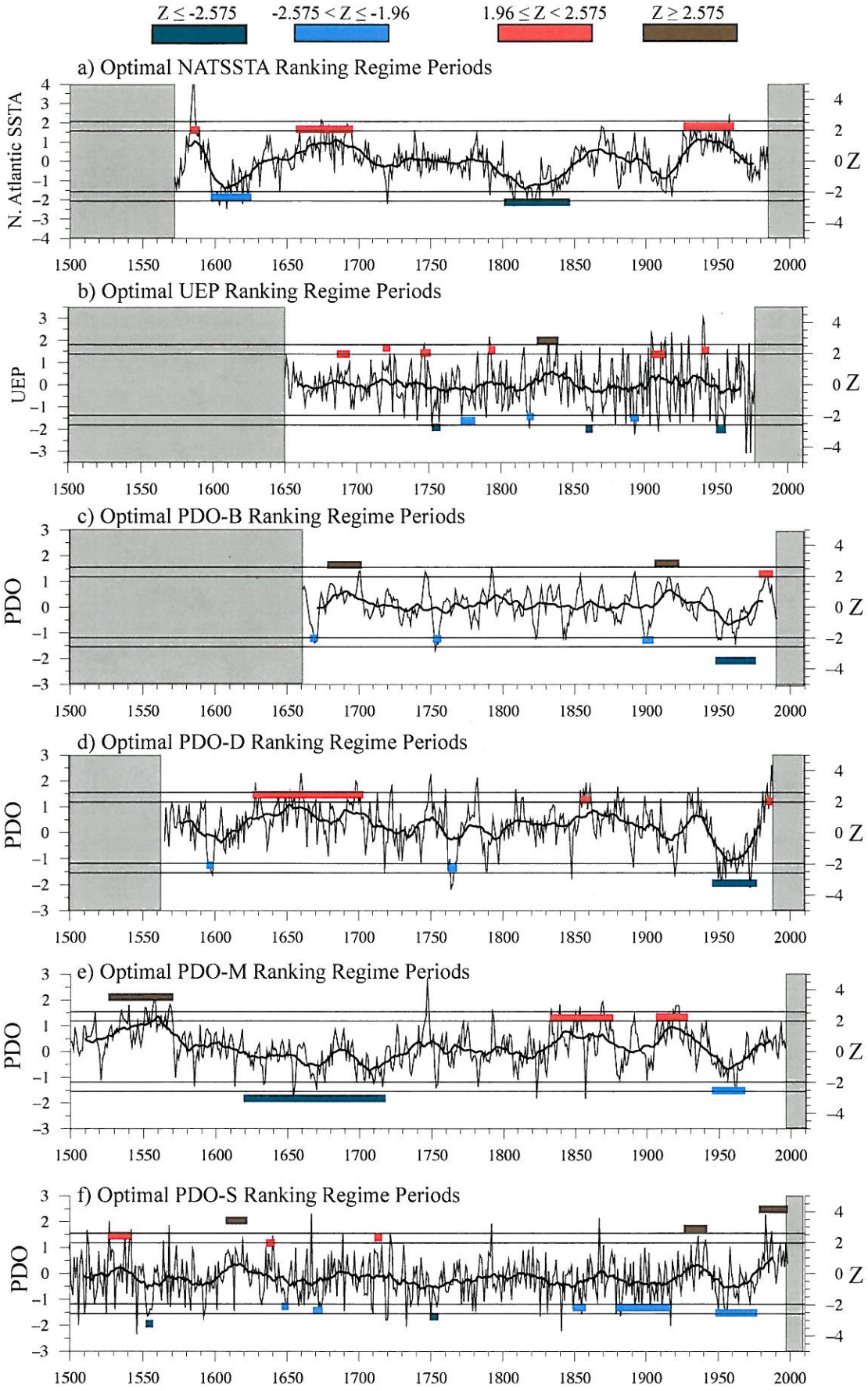

Figure A1. a) Optimal ranking regime analysis of the North Atlantic SSTA reconstruction of Gray et al. (2004). b) As in (a) for the Unified ENSO Proxy of McGregor et al. (2010). c) As in (a) for the PDO reconstruction of Biondi et al. (2001). d) As in (a) for the PDO reconstruction of D'Arrigo and Wilson (2006). e) As in (a) for the PDO reconstruction of MacDonald and Case (2005). f) As in (a) for the PDO reconstruction of Shen et al. (2006).

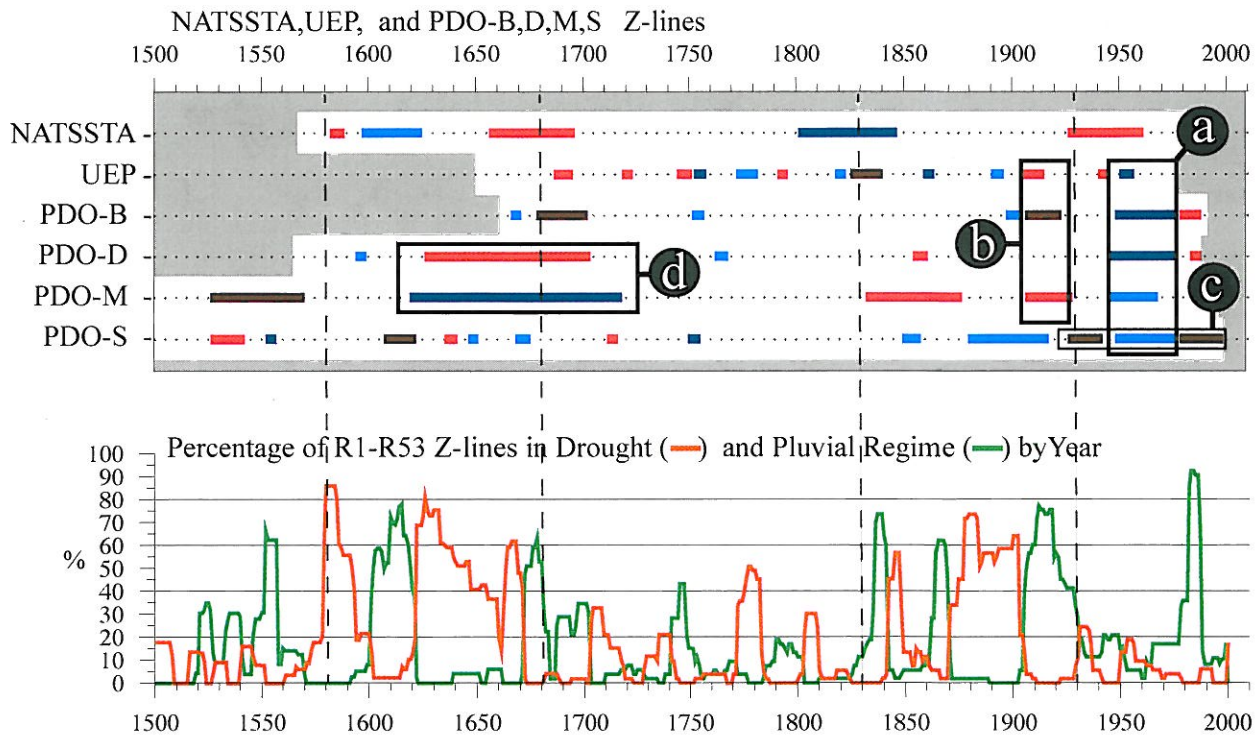

Figure A2. The optimal ranking regimes in Figs. A1e-f plotted as Z-lines. The significance shading scheme for Z statistics is as shown at the top of Fig. A1. The a-d black frames outline regime features discussed in the Appendix A text. The lower figure reproduces Fig. 4q, which shows the percentage of Fig. 4's R1-R53 Z-lines that indicate significant drought or pluvial conditions ($|Z| \geq 1.96$) during 500-2000. Green traces indicate the percentage of lines in a pluvial regime, and orange traces show the percentage of lines in a drought regime during each year.